Journal of Biogeography
April 2024, Volume 51, Issue 4, Pages 632-648
https://doi.org/10.1111/jbi.14774
https://archimer.ifremer.fr/doc/00866/97802/

Global genetic diversity and historical demography of the Bull Shark

Postaire Bautisse D. [1, *], Devloo-delva Floriaan [2, 3, 4, 5], Brunnschweiler Juerg M. [6], Charvet Patricia [7], Chen Xiao [8], Cliff Geremy [9, 10], Daly Ryan [11, 12], Drymon J. Marcus [13, 14], Espinoza Mario [15, 16], Fernando Daniel [17], Glaus Kerstin [18], Grant Michael I. [19], Hernandez Sebastian [20, 21], Hyodo Susumu [22], Jabado Rima W. [19, 23], Jaquemet Sébastien [1], Johnson Grant [24], Naylor Gavin J. P. [25], Nevill John E. G. [26], Pathirana Buddhi M. [17], Pillans Richard D. [27], Smoothey Amy F. [28], Tachihara Katsunori [29], Tillet Bree J. [30], Valerio-vargas Jorge A. [15], Lesturgie Pierre [31], Magalon Hélène [1], Feutry Pierre [2], Mona Stefano [31, 32]

[1] UMR ENTROPIE (Université de La Réunion/IRD/CNRS/IFREMER/Université de Nouvelle Calédonie), Université de La Réunion Saint Denis, France
[2] Environment, CSIRO Hobart Tasmania ,Australia
[3] Quantitative Marine Science, Institute for Marine and Antarctic Studies, University of Tasmania Hobart ,Australia
[4] Discipline of Biological Sciences, School of Natural Sciences University of Tasmania Hobart ,Australia
[5] National Research Collections Australia, CSIRO Hobart Tasmania ,Australia
[6] Independent Researcher Zurich ,Switzerland
[7] Programa de Pós-graduação em Sistemática, Uso e Conservação da Biodiversidade, Universidade Federal do Ceará (PPGSis - UFC) Fortaleza, Brazil
[8] College of Veterinary Medicine, South China Agricultural University Guangzhou ,China
[9] KwaZulu-Natal Sharks Board Umhlanga ,South Africa
[10] School of Life Sciences, University of KwaZulu-Natal Durban ,South Africa
[11] Oceanographic Research Institute, South African Association for Marine Biological Research Durban ,South Africa
[12] South African Institute for Aquatic Biodiversity Mkhanda, South Africa
[13] Coastal Research and Extension Center, Mississippi State University Biloxi Mississippi, USA
[14] Mississippi-Alabama Sea Grant Consortium Ocean Springs Mississippi, USA
[15] Centro de Investigación en Ciencias del Mar y Limnología & Escuela de Biología, Universidad de Costa Rica, San Pedro de Montes de Oca San José ,Costa Rica
[16] MigraMar, Sir Francis Drake Boulevard Olema California ,USA
[17] Blue Resources Trust Colombo, Sri Lanka
[18] School of Agriculture, Geography, Environment, Ocean and Natural Sciences, SAGEONS, The University of the South Pacific Suva, Fiji
[19] College of Science and Engineering, Centre for Sustainable Tropical Fisheries and Aquaculture, James Cook University Townsville ,Australia
[20] Biomolecular Laboratory, Center for International Programs, Universidad VERITAS San José, Costa Rica
[21] Sala de Colecciones, Facultad de Ciencias del Mar, Universidad Católica del Norte Coquimbo ,Chile
[22] Laboratory of Physiology, Atmosphere and Ocean Research Institute, University of Tokyo Kashiwa Chiba ,Japan
[23] Elasmo Project Dubai ,United Arab Emirates
[24] Department of Industry Trade and Tourism, Aquatic Resource Research Unit Darwin Northwest Territories ,Australia

[25] Florida Museum of Natural History, University of Florida Gainesville Florida ,USA
[26] Environment Seychelles Victoria ,Republic of Seychelles
[27] Environment, CSIRO Dutton Park ,Australia
[28] NSW Department of Primary Industries, Fisheries Research, Sydney Institute of Marine Science Mosman New South Wales, Australia
[29] Laboratory of Fisheries Biology and Coral Reef Studies, Faculty of Science, University of Ryukyus Nakagami Okinawa ,Japan
[30] Translational Research Institute, University of Queensland Diamantina Institute Brisbane ,Australia
[31] Institut de Systématique, Evolution, Biodiversité (ISYEB), Muséum National d'Histoire Naturelle, EPHE-PSL, Université PSL, CNRS, SU, UA Paris, France
[32] EPHE, PSL Research University Paris ,France

* Corresponding author : Bautisse D. Postaire, email address : postaireb@gmail.com

---

Abstract :

Aim

Biogeographic boundaries and genetic structuring have important effects on the inferences and interpretation of effective population size (Ne) temporal variations, a key genetics parameter. We reconstructed the historical demography and divergence history of a vulnerable coastal high-trophic shark using population genomics and assessed our ability to detect recent bottleneck events.

Location

Western and Central Indo-Pacific (IPA), Western Tropical Atlantic (WTA) and Eastern Tropical Pacific (EPA).

Taxon

Carcharhinus leucas (Müller & Henle, 1839).

Methods

A DArTcap™ approach was used to sequence 475 samples and assess global genetic structuring. Three demographic models were tested on each population, using an ABC-RF framework coupled with coalescent simulations, to investigate within-cluster structure. Divergence times between clusters were computed, testing multiple scenarios, with fastsimcoal. Ne temporal variations were reconstructed with STAIRWAYPLOT. Coalescent simulations were performed to determine the detectability of recent bottleneck under the estimated historical trend for datasets of this size.

Results

Three genetic clusters corresponding to the IPA, WTA and EPA regions were identified, agreeing with previous studies. The IPA presented the highest genetic diversity and was consistently identified as the oldest. No significant within-cluster structuring was detected. Ne increased globally, with an earlier onset in the IPA, during the last glacial period. Coalescent simulations showed that weak and recent bottlenecks could not be detected with our dataset, while old and/or strong bottlenecks would erase the observed ancestral expansion.

Main Conclusions

This study further confirms the role of marine biogeographic breaks in shaping the genetic history of large mobile marine predators. Ne historical increases in Ne are potentially linked to extended coastal habitat availability. The limited within-cluster population structuring suggests that Ne can be monitored over ocean basins. Due to insufficient amount of available genetic data, it cannot be concluded whether overfishing is impacting Bull Shark genetic diversity, calling for whole-genome sequencing.

Keywords : Carcharhinidae, coalescent simulations, DArTcap, demographic history, marine biogeography

Acknowledgments

Sampling permits and ethics approval are listed in Supplementary material 7. Bautisse D. Postaire was supported by a postdoctoral fellowship from the Laboratoire d'Excellence CORAIL, associated with the BULLGENE research project. We are grateful to the Genotoul bioinformatics platform Toulouse Midi-Pyrenees (Bioinfo Genotoul; http://bioinfo.genotoul.fr/) for providing computing resources. Floriaan Devloo-Delva was supported by a joint UTAS/CSIRO scholarship and the Quantitative Marine Science program. Sequencing was supported by the Sea World Research and Rescue Foundation Inc, the Ord River Research Offset grant through CSIRO, and the Marine Biodiversity Hub, a collaborative partnership supported through funding from the Australian Government's National Environmental Science Program. Samples from Reunion Island were collected as part of

projects EcoRecoRun and Eurraica funded by the DEAL/SEB. We would like to acknowledge Peter Kyne, Nicole Phillips, Lei Yang, William White, Jennifer Ovenden, Jessica Morgan, Thomas Poirout, Arie de Jong, Jeffrey de Pauw, Victor Peddemors, Betty Laglbauer, Blue Resources Trust, Beqa Adventure Divers, the operations and research staff of the KZN Sharks Board (SAF), and the many Traditional Owners, assistants, and volunteers for their help with obtaining samples from across the various research projects. We also like to thank all fishers and landing sites workers for their help in providing access to the sampled specimen.

Introduction

Three biogeographic boundaries have been promoting speciation in the marine realm since the early Neogene: the Eastern Tropical Pacific open ocean, the Benguela Current, and the Isthmus of Panama (Cowman & Bellwood, 2013; Lessios, 2008; O'Dea et al., 2016; Waters, 2008 . Their gradual formation has separated a once continuous tropical ocean linked through the Tethyan Seaway and several seaways, connecting current Western Tropical Atlantic (WTA) to the Western and Central Pacific (IPA) between the Triassic and the Pliocene (Hou & Li, 2018; Popov et al., 2004). On the eastern side of this ocean, the Eastern Pacific open ocean has been preventing eastward species colonization from the IPA to the Eastern Tropical Pacific (EPA) for at least 65 million years before present (B.P.; Cowman & Bellwood 2013). On its western side, the closure of the Tethyan Seaway at the end of the Middle Miocene (Sun et al., 2021) and the formation of the Benguela Current during the Pliocene (Jung et al., 2014) isolated the IPA from WTA. Finally, the formation of the Isthmus of Panama at the end of the Pliocene isolated the EPA from the WTA (O'Dea et al., 2016). These boundaries limited or stopped, geneflow between populations, impacting genetic structure and diversity. Known biogeographic breaks provide foundation to identify biodiversity patterns, but also help in delineating conservation regions when studying their effects on species connectivity (Fredston-Hermann et al., 2018; Norris, 2004).

Effective species' conservation and management require understanding of their population dynamics, biogeographical ranges, life history traits, and genetic connectivity (Green et al., 2014; Hohenlohe et al., 2021; Young et al., 2006). These factors shape temporal variations of population census and effective sizes (*Ne*). Census size is a parameter difficult to measure for vagile or rare species (Gerber et al., 2014) and it does not inform on adaptive potential (Reed & Frankham, 2016). Conversely, N_e and its temporal variation can be estimated using molecular markers. This ultimately enables an understanding of environmental or human induced factors influencing such variation, providing clues on adaptive potential and species management planning (Luikart et al., 2010; Nadachowska-Brzyska et al., 2021; Ouborg et al., 2010). However, N_e estimations require knowledge of the demographic history, as spatial structure influences N_e and may bias inferences (Arredondo et al., 2021; Chikhi et al., 2010; Lesturgie, Lainé, et al., 2022; Lesturgie, Planes, & Mona, 2022; Maisano Delser et al., 2019;

Mazet et al., 2016). Previous studies showed through theoretical and simulation arguments that incorrect modelling of population structure may lead to inaccurate historical demography interpretation n (Chikhi et al., 2010; Lesturgie, Lainé, et al., 2022; Lesturgie, Planes, & Mona, 2022; Maisano Delser et al., 2019; Wakeley, 2009).

Elasmobranchs are among the most threatened marine organisms (Dulvy et al., 2021). Many species exhibit late maturity, low fecundity, long gestation, and slow growth, making them susceptible to overfishing (Adams, 1980; Cortés, 2000). Moreover, the common reliance on nursery areas (Heithaus, 2005) and philopatric behavior (Chapman et al., 2015) increase the risk of local extinctions. Many modern elasmobranch groups predate the Tethyan closure, with this subclass probably already widely distributed by the Lower Jurassic (Maisey, 2012). Biogeographic barriers have different effects on elasmobranchs populations, mainly due to their reproductive ecology and physiology (Kottillil et al., 2023). While the Benguela Current is a strong barrier for many organisms (Teske et al., 2011), partial migration from the IPA to the WTA has already been documented in some sharks (Lesturgie, Lainé, et al., 2022; Lesturgie, Planes, & Mona, 2022). Strong barriers such as the Isthmus of Panama or the Eastern Pacific open ocean have promoted genetic differentiation and even speciation of shark populations (Gonzalez et al., 2021; Pazmiño et al., 2018). Based on mitochondrial DNA (mtDNA) data, coastal or demersal species tend to present genetic structuring at small geographic scales (Hirschfel et al., 2021; Momigliano et al., 2017; Vignaud et al., 2014) while pelagic or semi-pelagic species show low structuring between and within ocean basins (Bailleul et al., 2018; Pirog, Jaquemet, et al., 2019). Until recently, most elasmobranch genetic studies relied on traditional markers, *i.e.,* mtDNA and microsatellites (Phillips et al., 2021). These markers represent small portions of a genome, allowing only partial reconstructions of a species evolutionary history. Nowadays, the popularity of genotyping-by-sequencing (GBS) approaches has fueled genomic studies in non-model organisms (*e.g.,* Combosch & Vollmer, 2015; Harvey & Brumfield, 2015). However, few elasmobranchs have benefited yet (see Devloo-Delva et al., 2023; Feutry et al., 2020; Glaus et al., 2020; Lesturgie et al., 2023; Lesturgie, Lainé, et al., 2022; Lesturgie, Planes, & Mona, 2022; Maisano Delser et al., 2016, 2019; Pazmiño et al., 2018). Filling this gap will address several evolutionary questions and prompt refined conservation management plannings.

The Bull Shark *Carcharhinus leucas* (Müller & Henle, 1839) is an euryhaline, globally distributed, migratory species inhabiting tropical to warm temperate waters (Compagno, 1990). Earliest fossils of this species date 23 million B.P. and are present across what was the Tethys Sea, from Peru to the Mekong River (Gausmann, 2021). This species can travel along continental coasts (Espinoza et al., 2016, 2021; Heupel et al. 2015), into freshwater rivers (Werry et al., 2012), and across open ocean (Lea et al., 2015). Its trophic position in food webs, combined with its movement, make the species ecologically important. Females rely on coastal nurseries (Sandoval Laurrabaquio-Alvarado et al., 2019; Tillett et al., 2012) and some studies hypothesized a tendency for philopatry, based on telemetry and genetic data (Espinoza et al., 2016; Pirog, Jaquemet, et al., 2019). The Bull Shark evolutionary history has been investigated using traditional molecular markers (Karl et al., 2011; Pirog, Ravigné, et al., 2019; Sandoval Laurrabaquio-Alvarado et al., 2019; Testerman, 2014) and GBS data (Devloo-Delva et al., 2023; Glaus et al., 2020), but a detailed modeling of its N_e historical trajectory and the timing of divergence between inferred genetic clusters, is lacking. Moreover, N_e temporal trends and estimates are inconsistent, due to the limits and variety of molecular markers used to date (Karl et al., 2011; Pirog, Ravigné, et al., 2019; Sandoval Laurrabaquio-Alvarado et al.,

2019; Testerman, 2014). An assessment of current demographic trends is crucial, as populations have declined in the IPA (based on catch data). *Carcharhinus leucas* was recently assessed as Vulnerable by the International Union for the Conservation of Nature (IUCN) Red List of Threatened Species (Rigby et al., 2021). This decline is probably due to overfishing, as it is among the most traded species (Cardeñosa et al., 2018, 2022; Cardeñosa, Fields, et al., 2020; Cardeñosa, Shea, et al., 2020; Fields et al., 2018).

The present study aims to: (1) identify the most likely evolutionary divergence scenario that may have shaped the observed genetic structure of *C. leucas*; (2) reconstruct the historical variation of N_e in the identified clusters, and (3) test whether recent bottlenecks could be detected given the observed genetic diversity and sample sizes in this study. Results will inform management and conservation actions by providing a first estimate of *C. leucas* N_e and its historical trend on a global scale while assessing our ability to monitor N_e with the available genomic data.

Material and methods

Sample collection and DNA extraction

A subsample of the dataset of Devloo-Delva et al. (2023) was used for this study, representing 475 *C. leucas* sampled between 1985 and 2019 from 18 locations covering its distribution (except for West Africa; Supplementary Material 1). DNA was extracted with the Qiagen Blood and Tissue kit, following standard protocol (Qiagen Inc., Valencia, California, USA). After bait design and bioinformatic filtering (see following sections), the dataset comprised 16 sampling locations with at least five individuals (309 individuals; Fig. 1, Table 1) covering the WTA, IPA, and EPA. Sampling locations with mostly adults were preferentially selected to limit relatedness effects.

SNP selection for bait design

The approach used for bait design is described in Devloo-Delva et al. (2023). Briefly, a subset of 219 sample libraries were genotyped using the DArTseq™ approach (Cruz et al., 2013; Feutry et al., 2017, 2020, Supplementary material 1). From this dataset, 3,400 loci of 70 bp were randomly selected for DNA-capture bait development. The DArTcap™ enriched libraries were sequenced on a Illumina HiSeq 2500.

Bioinformatics

Reads were demultiplexed with DArTsoft14™ and analyzed using STACKS 2.5 (Rochette et al., 2019). STACKS clustering parameters were optimized as recommended by Paris et al. (2017). First, the *denovo* pipeline was run on a randomly selected sampling site (Seychelles) with different combinations of *m* (minimum number of raw reads to form a stack; from 3 to 10), *M* (number of mismatches between stacks within an individual to merge stacks; set to 4, 6, or 8), and *n* (number of mismatches between stacks in different individuals; equal to *M*). The number of polymorphic loci, SNPs, the nucleotide diversity θ_π, and θ_w (Watterson, 1975) were compared between parameter combinations, allowing up to 20% of missing data per locus. We selected the parameters $m = 3$, $M = 4$, and $n = 4$ which maximized the number of loci retrieved without over-splitting the dataset. Using these parameters, the *denovo* pipeline was run on individuals belonging to sampling locations with more than five individuals. Loci were

first filtered using the *population* function to discard: (i) SNPs with heterozygosity rate > 0.8; and (ii) SNPs with more than 20% missing data in any sampling site. Finally, we filtered the dataset with a custom R script (R Core Team, 2022) to discard: (i) loci with more than five SNPs (after checking the empirical distribution of SNPs per locus); (ii) SNPs with average coverage < 10X or > 60X (after checking the empirical distribution); and (iii) individuals with more than 10% missing data.

Additional filters were applied, depending on downstream analyses. To analyze population genetic structure, one random SNP per locus was retained (to avoid linkage disequilibrium) with a minor allele frequency > 0.05 (hereafter, the *global* dataset). To estimate the genetic diversity in each population and model historical demography, all SNPs without missing data were retained (called *population* dataset).

Population structure

As this study uses a subset of an existing dataset (Devloo-Delva et al., 2023), standard population structure analyses were performed to assess the concordance and robustness of previous results.

The global genetic structure was evaluated using a hierarchical approach in fastSTRUCTURE 1.0 (Raj et al., 2014). For the *global* dataset and each sub-dataset, three independent runs were performed with *K* varying between 1 and 10. This was performed until no sub-clustering was detected (*i.e,* optimal $K = 1$). The expected admixture proportions inferred by fastSTRUCTURE were visualized with DISTRUCT (Rosenberg, 2004).

Population clustering was further investigated using a Discriminant Analysis of Principal Component (DAPC) with the 'adegenet' R package (Jombart, 2008). The decrease in Bayesian information criterion (BIC) values was examined to identify the optimal *K* (Jombart et al., 2010). The *dapc* function was executed using the chosen *K* value, retaining the axes of PCA explaining ≥ 80% of the total variance. Pairwise fixation indices (F_{ST}; Reynolds et al., 1983) between sampling locations were calculated using the 'diveRsity' R package (Keenan et al. 2013), with significance tested after 1,000 permutations.

Demographic inferences

Historical demography was explored using the STAIRWAYPLOT 2.0 (Liu & Fu, 2020). The STAIRWAYPLOT models the folded site frequency spectrum (SFS) to infer coalescence rate changes through time. If individuals come from a panmictic population, the coalescence rate can be converted to N_e using a generation time and a mutation rate. We applied a generation time of 13 years, computed as the average age of sexual maturity of 15 years in the Atlantic (Branstetter & Stiles, 1987) and ~12 years in the Indian Ocean (Hoarau et al., 2021). It should be noted that this arbitrary value represents the minimal age at which an individual could contribute to the genetic diversity of the next generation [the IUCN reports a generation time of 22.7 years (Rigby et al., 2021)]. We applied the mutation rate estimated by Lesturgie, Planes, & Mona, (2022) based on *Carcharhinus melanopterus* RAD-seq data after scaling it to account for the generation time of *C. leucas*. This resulted in a mutation rate of 2.509×10^{-8} per site per generation.

Population structure can bias the estimation of temporal N_e variation based on models assuming panmixia (Chikhi et al., 2010; Lesturgie, Lainé, et al., 2022; Lesturgie, Planes, & Mona, 2022; Maisano Delser et al., 2019; Wakeley, 2009). It is therefore important to test for population structuring before interpreting the reconstructed N_e. The approach proposed by Lesturgie, Planes, & Mona, (2022) was used in addition to the clustering analyses. We devised three demographic models to test if the summary statistics observed in each sampling location (deme) are more likely to be described by an unstructured model (*i.e.,* a panmictic population) or a meta-population represented by an array of demes exchanging migrants either under a finite island or a steppingstone model. Each deme was analyzed separately, and the probability of each of the three model is evaluated using an approximate Bayesian computation (ABC) framework. This approach has been shown to capture major features of the gene genealogy of a sample of lineages, *i.e.,* if they originate from a single panmictic deme or from a deme belonging to a meta-population (Peter et al. 2010, Maisano Delser et al. 2019).

The non-structured model (NS) represents a modern population of constant size N_{mod} switching instantly to an ancestral population of size N_{anc} at T_c generations in the past. The finite island model (FIM) represents an array of 100 demes each with constant size N_{mod} and exchanging N_{mig} migrants per generation (lineages were sampled from one random deme of the array); backward in time, all demes merged instantaneously at T_c generations ago into a single population of size N_{anc}. The stepping-stone model (SST) resembles FIM, the difference being that populations only exchange migrants with their four closest neighbors and the lineages were sampled from one of the central demes of the array (Supplementary material 2). A total of 50,000 coalescent simulations for each model were performed with *fastsimcoal* 2.7.05 (Excoffier et al., 2013), extracting parameters from prior distributions (Table 1). Each sampling site was analyzed separately, and simulations reproduced the exact number of individuals and loci observed in its corresponding *population* dataset. Model election and parameter estimations were based on the following set of summary statistics: the folded SFS, θ_π, θ_w, TD (Tajima, 1989) and the number of segregating sites (S). Summary statistics were considered for both model selection and parameter estimation. Model selection was performed using the Random Forest (RF) classification approach implemented in the 'abcRF' R package (Pudlo et al., 2016). RF were trained using the simulated datasets, represented by the vector of summary statistics. The observed data were then assigned to one of the three model. We considered the model assignment reliable if its probability was > 0.5. The demographic parameters of the best model were then estimated with the 'abcRF' regression method (Raynal et al., 2019). The number of trees of each RF algorithm was chosen by monitoring the out-of-bag error (Pudlo et al., 2016). A Confusion Matrix was also generated during the model selection procedure to determine its performance: simulated datasets were assigned to one of the three models under investigation following the same procedure applied to the observed data. This allows a test the of robustness of our procedure within the space of prior parameters chosen.

Simulation study – Detection of recent bottleneck

The detectability of recent bottlenecks (5 to 1,500 generations) was explored by running the STAIRWAYPLOT on simulated datasets having a number of individuals and loci consistent with the *population* datasets (see below). We focused on recent bottlenecks in populations experiencing a demographic history consistent with the one reconstructed here. According to our results, the demographic trajectories for most sampling locations could be described by a

NS model with an ancestral N_e of 5,000 individuals switching 6,000 generations ago to a modern N_e of 16,000 individuals. These values were based on averages taken from both the STAIRWAPLOT and ABC-RF results at sampling locations for which the NS model had a posterior probability > 0.5. *fastsimcoal* was used to run coalescent simulations under this NS model to which an instantaneous bottleneck was added (hereafter, NS_{BOT} model). Two hundred and four scenarios were investigated (Table 3, Supplementary material 3), combining variations in: (i) number of sampled individuals (5, 10, 15 or 20); (ii) number of sampled independent loci (1,000, 5,000 or 10,000 loci of 100 bp); (iii) onset of the bottleneck (called T_{BOT}) in number of generations ago, taking values of 0, 5 [65 B.P., the beginning of industrial fishing (Mansfield, 2010)], 50 (650 B.P., an intermediate value within the last millennium), 450 [5,850 B.P., the end of the Holocene Climate Optimum (Summerhayes & Charman, 2015)] and 1,500 [19,500 B.P., the end of the Last Glacial Maximum (LGM; Clark et al., 2009)]; (iv) strength of the bottleneck (called BOT) which was set to decrease modern N_e 0, 5, 10, 50 or 100 times. Ten simulations were replicated per parameters combination and the same summary statistics as in the real data (θ_π, θ_w, TD, and S) were computed. STAIRWAYPLOT was then run on all replicates and the average of the estimated values were plotted.

Ancestral divergence

fastsimcoal was used to investigate the timing of divergence among the three main biogeographic regions (*i.e.,* WTA, EPA, IPA), corresponding to the three genetic clusters identified (see results and Supplementary Material 6), in agreement with Devloo-Delva et al. (2023). This method uses a composite likelihood approach to optimize population demographic parameters under a defined scenario. The likelihood is computed by comparing the observed SFS to the one expected given a specific combination of demographic parameters, which is obtained by means of coalescent simulations. To maximize the number of loci without missing data and obtain a balanced sampling for each region, 15 individuals were randomly sampled from each genetic cluster (the U.S. Atlantic coast population was excluded to use individuals sampled on the same time frame), hereafter the *divergence* dataset. We used identical filters as for other historical demographic analyses and we calculated the pairwise folded two-dimensional SFS (2D-SFS). Twenty-two scenarios were tested (Supplementary material 4). First, we tested the most likely population tree topology *i.e.,* a synchronous or a sequential divergence between the genetic clusters (Fig. 2). Then, we tested for continuous (symmetrical or asymmetrical) gene flow among clusters for the best population tree topology. We further tested the likelihood of a secondary contact between EPA and WTA after a complete isolation, potentially initiated by the opening of the Panama Canal around eight generations ago. The secondary contact model was tested within all tree topologies.

The likelihood of each scenario and its parameter values was assessed after selecting the best of 100 independent runs. The likelihood was evaluated by 250,000 simulations for each parameter combination and maximized by implementing 50 Expectation-Conditional-Maximization cycles (Meng & Rubin, 1993). The range of modern and ancestral N_e (N_e and N_{anc}, Fig. 2) was bounded between 50 to 50,000 individuals for each cluster. Divergence times (T_x, Fig. 2) ranged between 100 and 100,000 generations (1,300 to 1,300,000 B.P). Per generation migration rates was investigated between 10^{-7} and 0.01. *fastsimcoal* can explore values beyond boundaries if the likelihood increases. The run with the highest likelihood within each scenario was extracted to perform model selection using the Akaike Information

Criterion (AIC). Parameters' confidence intervals were calculated with a parametric bootstrap approach: 100 datasets were simulated using the maximum likelihood values of the best scenario, then the 2D-SFS was computed for each pair of population comparisons. Finally *fastsimcoal* was run on each of these replicates with the same condition as for the real data. The best run out of 100 for each replicate was chosen to build the final confidence interval.

Results

Genotyping of DArTcap data and datasets

After filtering, 734 polymorphic loci were recovered from the *global* dataset, with a mean read depth of ~37x (s.e. = 0.11) per locus. Between 558 and 1,167 (mean ± s.e. = 938.82 ± 61.24) SNPs per sampling site were obtained in the *population* datasets (Table 1), with a mean read depth per locus per sampling site ranging from 24.50x (s.e. = 0.15) in Costa Rica to 28.13x (s.e. = 0.14) in South Africa. Finally, 715 polymorphic loci were obtained in the *divergence* dataset, with a mean depth of 25.81x (s.e. =0.29) per locus.

Population clustering and genetic connectivity

Strong genetic differentiation was identified between IPA, WTA, and EPA. fastSTRUCTURE analyses suggested $K = 2$ as the best number of clusters for the *global* dataset (Supplementary Material 6a): WTA and EPA individuals clustered together and the IPA formed a second cluster. When analyzing only WTA and EPA, fastSTRUCTURE identified two genetic clusters, matching the individuals' biogeographic origin. No further sub-clustering was detected within these regions. EPA was not run alone as it consists of a single sampling location. DAPC did not identify a single best solution according to the BIC, but its visual inspection suggested K equal to 2 or 3 as the most likely values (Supplementary Material 6b), consistent with fastSTRUCTURE. For $K = 2$, DAPC identified one cluster with only IPA individuals and the other one with WTA + EPA individuals. For $K = 3$, the first axis separated the WTA and EPA individuals from the IPA, while the second axis segregated individuals from the EPA, explaining > 95% of the total variance.

The analysis of molecular variance computed using the three biogeographic regions as groups (in agreement with the clustering results) revealed that 54.81% of the total variance is partitioned in the between-region component ($P < 0.005$), compared to 1.01% ($P < 0.005$) in the between-sampling locations within regions component. The remaining genetic variation was found within sampling locations (45.2%, $P < 0.005$).

All pairwise differentiation tests between sampling locations from different biogeographic regions showed significant F_{ST} values (range: 0.33-0.69). The mean genetic differentiation between sampling locations from the EPA and WTA (mean $F_{ST} = 0.36$, range: 0.33-0.39) was lower than the mean differentiation between sampling locations from the IPA and the other two biogeographic regions (IPA vs. EPA mean $F_{ST} = 0.62$, range: 0.56-0.69; IPA vs. WTA mean $F_{ST} = 0.61$, range: 0.54-0.66). Within the WTA, the pairwise F_{ST} values indicated significant differentiation between sampling locations (mean $F_{ST} = 0.01$, range: 0.005-0.013), with the U.S. Atlantic coast isolated from the northern Gulf of Mexico and Brazil (mean $F_{ST} = 0.012$). In the IPA, all pairwise differentiation tests between Fiji (FIJ) and other sampling locations were significant (mean $F_{ST} = 0.036$, range: 0.026-0.075), as well as comparisons between Iriomote Island (IRI) in Japan and other sampling locations (mean $F_{ST} = 0.044$, range: 0.038-0.050).

Among the other pairwise differentiation from the IPA, most were not significant with F_{ST} values indicating negligible genetic differentiation (mean F_{ST} = 0.003, range: 0-0.011; Table 2), without clear geographic signal.

Demographic inferences

Summary statistics are presented in Table 1. TD were negative in all sampling locations, indicating an excess of low frequency variants. According to the ABC-RF framework, the NS model had a posterior probability > 0.5 in 10 sampling locations (one in the WTA and nine in the IPA; Table 1). The 95% credible intervals of T_{col} and N_{anc} for FIJ and IRI mostly overlapped prior distributions, suggesting that the data does not contain enough information to correctly estimate model parameters. Other IPA sampling locations showed N_e increase (mean N_{mod}/N_{anc} ratio ± s.e. = 3.65 ± 0.48) occurring around ~110,000 B.P., switching from a mean N_{anc} of ~5,000 individuals to a mean N_{mod} of ~19,000 individuals. The parameter estimation of the NS model for the WTA sampling site gave a similar pattern to most IPA sampling locations, with N_{anc} being approximately one third of N_{mod}.

Demographic trajectories reconstructed with STAIRWAYPLOT (interpreted as N_e temporal variation because panmixia could not be rejected in most cases) were consistent with the ABC-RF results. The difference in the timing of the expansion stems from the fact that STAIRWAYPLOT implements a non-parametric N_e variation model, while the ABC-RF framework employs a single N_e time change. For all sampling locations except IRI, an increase of median N_e was observed, starting ~20,000-60,000 B.P. in WTA populations (Fig. 3a), while ~60,000-80,000 B.P. in most of the IPA sampling locations (Fig. 3c and Fig. 3d), with Thailand being the oldest. Since then, a comparatively constant median N_e was observed (Fig. 3) until a generalized reduction in recent generations. Three sampling locations from the IPA depart from this pattern: FIJ, IRI and Sydney (Fig. 3d). FIJ and Sydney sampling locations fit the general template but with a younger expansion starting ~20,000 B.P. IRI does not present any ancestral expansion, only N_e reduction in the last millennia.

Simulation study – Detection of recent bottleneck

Coalescent simulations run under the NS model reproduced the genetic variability observed in real populations (Table 3, Supplementary Material 3), and the simulated trajectory was generally well retrieved by the STAIRWAYPLOT (Supplementary Material 5a), particularly when increasing the number of loci and sampled individuals. The STAIRWAYPLOT run on datasets simulated under the NS model presented a reduction of median N_e in the most recent (~10) generations when analyzing 1,000 to 5,000 loci, as observed in real data (Fig. 4a, Supplementary Material 5a). This reduction disappeared when analyzing more loci (Fig. 4, Supplementary Material 5). For scenarios simulated under NS_{BOT}, the STAIRWAYPLOT could recover a recent bottleneck (T_{BOT} = 5) only for large N_e reduction (BOT > 50x), showing a decreasing trajectory in recent generations (Figure 5b-e, Supplementary material 3b). In contrast, STAIRWAYPLOT reconstructed the decreasing N_e trajectory at all BOT intensities when datasets were simulated with older T_{BOT}. However, STAIRWAYPLOT progressively failed to recover the ancestral N_e expansion included in all scenarios as BOT and T_{BOT} values increased. For older (T_{BOT} = 450 and 1,500) and/or strongest bottlenecks (BOT > 10x, Supplementary Material 5d-e), the demographic history was dominated by the post-bottleneck coalescence rate: the STAIRWAYPLOT reconstructed populations with constant N_e corresponding to the

post-bottleneck value (looking forward in time). For T_{BOT} = 1,500 and BOT > 50x, almost all genetic diversity was lost and STAIRWAYPLOT could not reconstruct N_e trajectories over more than a few generations.

Ancestral divergence

Model selection identified the scenario of an ancestral divergence of IPA as the most likely (Fig 2 - Model 2, Supplementary Material 4). Within this topology, we found that the model with highest support displayed continuous asymmetrical migration rates between genetic clusters (Table 4). According to this model (Table 4), the estimated divergence time between the WTA and EPA was ~40,000 B.P., and ~56,000 B.P. between IPA and the ancestor of the EPA and WTA genetic clusters. IPA estimated modern N_e closer to other demographic inferences performed in this study (~14,500 individuals), to the contrary of the other two clusters which presented lower N_e estimates (EPA = ~7,500 and WTA = ~3,500). Similarly, ancestral N_e were small, below 300 individuals in both cases. Migration rates were extremely low, less than one individual per generation in all cases. IPA estimated modern N_e falls outside its 95% bootstrap confidence interval, as did the estimated divergence time between IPA and the ancestor of EPA and WTA. This indicated a lack of power to infer these parameters values with confidence.

Discussion

Previous studies have used microsatellites, mtDNA or genomic markers to uncover the mechanisms driving gene flow in *C. leucas* (Devloo-Delva et al., 2023; Glaus et al., 2020; Pirog, Ravigné, et al., 2019; Testerman, 2014). These studies underlined the weak and/or non-significant genetic differentiation between sampling locations inside biogeographic regions, while suggesting a strong disjunction among them. However, reconstruction accuracy increases with the number of independent loci analyzed (Felsenstein, 2006; Nordborg, 2019; Wakeley, 2009) and a representative sampling across the biogeographic range, which helps refine our understanding of the evolutionary history of the Bull Shark.

***Carcharhinus leucas* biogeography**

The present study supports the importance of biogeographic barriers in the diversification of *C. leucas* (Devloo-Delva et al., 2023). According to our estimations, the divergence of the IPA from the WTA and EPA occurred ~55,000 B.P., while the divergence between the WTA and EPA occurred ~40,000 B.P. It is worth noting that Pirog, Ravigné, et al., (2019) timed the divergence of IPA and WTA at ~1.23 million B.P. using mtDNA, linking it to the formation of the Benguela Current. The difference in the estimated divergence dates with the known insurgence of biogeographic barriers, *i.e.,* the Isthmus of Panama, the Benguela Current and the Eastern Pacific open ocean, is difficult to reconcile. While the Benguela Current is a permeable barrier (Bernard et al., 2018; Lesturgie, Lainé et al., 2022; Reid et al., 2016), the divergence between EPA and WTA after the closure of the Isthmus of Panama is surprising (but see Galván-Quesada et al., 2016). Indeed, low water temperatures form a thermal barrier to *C. leucas* around the southern and northern tips of the American continent since millions of years. Two scenarios could explain this discrepancy . The first is a secondary contact between EPA and WTA, artificially decreasing their divergence time via genomic introgression. To test this hypothesis, secondary contact scenarios were added to *fastsimcoal* modeling under the hypothesis that the opening of the Panama Canal fueled migration between ocean basins. However, the

likelihood of these models was lower (Supplementary Material 4) and the estimated divergence was still too recent (data not shown). A second explanation is that the mutation rate used here was two orders of magnitude higher than the real one. It seems unlikely that *C. leucas* would have such a slow mutation rate (around 10^{-10} per site per generation), which would be the lowest documented so far in vertebrates. Ultimately, our set of loci represented a fraction of the nuclear genome and in some cases the parameter estimates fell outside the confidence intervals, therefore the estimates should be taken cautiously. However, this does not affect the model selection procedure. Whole genome sequencing will certainly help refine our estimates.

Population structuring

This study further confirms that *C. leucas* is divided in at least three stocks (Olver et al., 1995) corresponding to major marine biogeographic regions: WTA, EPA, and IPA. Indeed, all analyses showed that while there is high gene flow within regions, they are almost completely genetically isolated. The lack of genetic differentiation inside regions is probably related to *C. leucas* ecology, as it is capable of moving thousands of kilometers along continents (Espinoza et al., 2016, 2021) and in the open ocean (Lea et al., 2015). However, two IPA locations stood out: FIJ and IRI. Devloo-Delva et al. (2023) and Glaus et al. (2020) identified FIJ as genetically distinct from other IPA locations, the latter suggesting that it resulted from the archipelago's oceanic isolation. However, FIJ was not the only isolated sampling location; Seychelles is ~1,000 km apart from Madagascar, yet it did not show traces of genetic isolation. Sampling bias could explain FIJ genetic differentiation, as most samples used here came from intermittently resident females suspected to pup in the area (Bouveroux et al., 2021; Brunnschweiler & Barnett, 2013; Cardeñosa et al., 2017; Glaus et al., 2019). Given the suspected reproductive philopatric behavior of *C. leucas* females (Devloo-Delva et al., 2023; Espinoza et al., 2016; Pirog Ravigné, et al., 2019), the Fijian genetic distinctiveness could stem from relatedness, as in Lemon sharks (Feldheim et al., 2014). Likewise, samples from Iriomote Island originate from a river used as nursery, with most individuals sampled younger than two years old (data not shown). However, if the genetic isolation came from higher relatedness, we would expect strong and positive F_{IS} values, which were not observed anywhere (Supplementary material 1). Ultimately, we could not exclude the presence of undiscovered biogeographic barriers, or that the high differentiation of populations at the edge of the species distribution is due to a recent range expansion. Sampling the northern IPA and Micronesia would determine whether the pattern corresponds to actual biogeographical borders or sampling artifacts (Gausmann, 2021). The genetic differentiation between the U.S. Atlantic coast and other WTA sampling locations could result from a biogeographic border, as the Florida Peninsula forms a barrier between the Gulf of Mexico and the Atlantic (Hirschfeld et al., 2021). A temporal effect could also play part in the distinction of this population (some samples were collected between 1984 and 1987).

Sharks life history traits largely affects population structure (Lesturgie, Lainé, et al., 2022; Lesturgie, Planes, & Mona, 2022), but few species have been studied on a global scale with genomic datasets similar to the one presented here. Species exhibiting strict fidelity to coral reef such as the Blacktip Reef and Grey Reef sharks present strong genetic structuring over the Indo-Pacific (Lesturgie et al. 2023, Maisano Delser et al. 2019). On the contrary, Tiger Shark, presenting a similar circumtropical distribution to *C. leucas*, is divided in two almost independent panmictic stocks (the Atlantic and the Indo-Pacific, Lesturgie, Lainé, et al., 2022). More species with similar distribution and such extensive geographic coverage need to be

studied to better understand the relationship between life history traits and genetic structuring.

Demographic history and effective population size

C. leucas global N_e increased during the last glacial period. During this period, sea levels were at least 50 m below present, extending coastlines and so the available habitat for *C. leucas* (Carlson et al., 2010; Graham et al., 2016; Hammerschlag et al., 2012; Heupel et al., 2015; Niella et al., 2020), potentially supporting larger populations. As *C. leucas* inhabits areas with water temperatures down to 18°C (Brunnschweiler et al., 2010; Lea et al., 2015; Matich & Heithaus, 2012; Smoothey et al., 2016, 2019, 2023), sea surface temperature changes during the LGM did not significantly reduce its distribution in the tropics (Monteagudo et al., 2021). Additionally, long-range movements (Espinoza et al., 2016; Lea et al., 2015; Lee et al., 2019) may have facilitated colonization of newly emerged areas. However, if available habitat was the sole driver of N_e, a reduction should have been observed after the LGM, as available coastal habitats receded. The ability to detect bottlenecks depends on many factors: intensity, timing, ancestral demography, and the number of individuals and loci sampled. In addition, recent population declines are harder to detect for long-lived and late maturing species, as fewer generations have elapsed in the same amount of time (*e.g.,* Roman & Palumbi 2003). Our simulations under the NS_{BOT} model suggested that even a limited N_e reduction starting during the mid-Holocene or the LGM (Supplementary material 5d-e) would have hidden the ancestral expansion retrieved in our populations, and it is therefore inconsistent with *C. leucas* evolutionary history. Conversely, our dataset does not have enough power to detect recent N_e reduction, at least with the use of the folded SFS. Indeed, the small decrease observed in the recent generations is most likely an artifact (Supplementary material 5a). In the future, it will be important to complement SFS-based methods with those based on linkage disequilibrium statistics, better suited to detect recent changes in N_e (Boitard et al, 2016; Kerdoncuff, Lambert & Achaz, 2020; Santiago et al., 2020) and to develop full genome resources.

Perspective of *C. leucas* populations conservation and management

Based on this study and complementing previous findings (Devloo-Delva et al., 2023; Pirog, Ravigné, et al., 2019), *C. leucas* from the IPA, WTA and EPA form three independent genetic clusters, and should considered as independent stocks following Olver, Shuter, & Minns (1995). Demographic modelling showed that the species still harbors significant genetic diversity, globally retaining its evolutionary potential, according to Frankham et al. (2014). Interestingly, the IPA seemed to be the oldest cluster, harboring the highest genetic diversity and likely be the center of origin of this species. Two important results are highlighted by our simulations: (i) decrease in N_e after the LGM or mid-Holocene can be excluded, as it would have shown a detectable signature on the observed genetic variation; (ii) conversely, a bottleneck starting five generations ago is undetectable with a dataset of this size, unless its strength approaches extreme values (Fig. 4, Supplementary material 5b). The ongoing population depletion in the IPA may not be recovered using the panel of loci analyzed here. In conclusion, even though elasmobranch populations have been following a downward trend for several decades (Dulvy et al.,2021; Pacoureau et al., 2021), its impact on the genetic diversity of this species requires more genomic data and the application of linkage disequilibrium-based statistics to be detectable.

References

Adams, P. B. (1980). Life history patterns in marine fishes and their consequences for fisheries management. *Fishery Bulletin*, 78(1), 1–12.

Arredondo, A., Mourato, B., Nguyen, K., Boitard, S., Rodríguez, W., Noûs, … Chikhi, L. (2021). Inferring number of populations and changes in connectivity under the n-island model. *Heredity*, 126(6), 896–912.

Bailleul D., Mackenzie A., Sacchi O., Poisson F., Bierne N., Arnaud-Haond S. (2018). Large-scale genetic panmixia in the blue shark (Prionace glauca): A single worldwide population, or a genetic lag-time effect of the "grey zone" of differentiation? Evolutionary Applications, 11, 614–630.

Bernard, A. M., Richards, V. P., Stanhope, M. J., & Shivji, M. S. (2018). Transcriptome-derived microsatellites demonstrate strong genetic differentiation in pacific white sharks. *Journal of Heredity*, 109(7), 771–779.

Boitard, S., Rodríguez, W., Jay, F., Mona, S., & Austerlitz, F. (2016). Inferring population size history from large samples of genome-wide molecular data - an Approximate Bayesian Computation approach. *PLoS Genetics*, 12(3), e1005877

Bouveroux, T., Loiseau, N., Barnett, A., Marosi, N. D., & Brunnschweiler, J. M. (2021). Companions and casual acquaintances: the nature of associations among bull sharks at a shark feeding site in Fiji. *Frontiers in Marine Science*, 8, 1–11.

Branstetter, S., & Stiles, R. (1987). Age and growth estimates of the bull shark, *Carcharhinus leucas*, from the northern Gulf of Mexico. *Environmental Biology of Fishes*, 20(3), 169–181.

Brunnschweiler, J. M., & Barnett, A. (2013). Opportunistic visitors: long-term behavioural response of bull sharks to food provisioning in Fiji. *PLoS ONE*, 8(3), e58522.

Brunnschweiler, J. M., Queiroz, N., & Sims, D. W. (2010). Oceans apart? Short-term movements and behaviour of adult bull sharks *Carcharhinus leucas* in Atlantic and Pacific Oceans determined from pop-off satellite archival tagging. *Journal of Fish Biology*, 77(6), 1343–1358.

Cardeñosa D., Fields A.T., Babcock E.A., Shea S.K.H., Feldheim K.A., Chapman D.D. (2020). Species composition of the largest shark fin retail-market in mainland China. *Scientific Reports*, 10, 1–10

Cardeñosa D., Fields A.T., Babcock E.A., Zhang H., Feldheim K., Shea S.K.H., Fischer G.A., Chapman D.D. (2018) CITES-listed sharks remain among the top species in the contemporary fin trade. *Conservation Letters,* 11, 1–7.

Cardeñosa D, Glaus K.B.J, Brunnschweiler J.M. (2017) Occurrence of juvenile bull sharks (Carcharhinus leucas) in the Navua River in Fiji. *Marine and Freshwater Research*, 68,592–597.

Cardeñosa D., Shea K.H., Zhang H., Feldheim K., Fischer G.A., Chapman D.D. (2020). Small fins, large trade: a snapshot of the species composition of low-value shark fins in the Hong Kong markets. *Animal Conservation*, 23, 203–211.

Cardeñosa D., Shea S.K., Zhang H., Fischer G.A., Simpfendorfer C.A., Chapman D.D. (2022) Two thirds of species in a global shark fin trade hub are threatened with extinction: Conservation potential of international trade regulations for coastal sharks. *Conservation Letters,* 15, 1–11.

Carlson, J. K., Ribera, M. M., Conrath, C. L., Heupel, M. R., & Burgess, G. H. (2010). Habitat use and movement patterns of bull sharks *Carcharhinus leucas* determined using pop-up satellite archival tags. *Journal of Fish Biology*, 77(3), 661–675.

Chapman, D. D., Feldheim, K. A., Papastamatiou, Y. P., & Hueter, R. E. (2015). There and back again: a review of residency and return migrations in sharks, with implications for population structure and management. *Annual Review of Marine Science*, 7(1), 547–570.

Chikhi, L., Sousa, V. C., Luisi, P., Goossens, B., & Beaumont, M. A. (2010). The confounding effects of population structure, genetic diversity and the sampling scheme on the detection and quantification of population size changes. *Genetics*, 186(3), 983–995.

Clark, P. U., Dyke, A. S., Shakun, J. D., Carlson, A. E., Clark, J., Wohlfarth, B., … McCabe, A. M. (2009). The Last Glacial Maximum. *Science*, 325(5941), 710–714.

Combosch, D. J., & Vollmer, S. V. (2015). Trans-Pacific RAD-Seq population genomics confirms introgressive hybridization in Eastern Pacific *Pocillopora* corals. *Molecular Phylogenetics and Evolution*, 88, 154–162.

Compagno, L. J. V. (1990). Alternative life-history styles of cartilaginous fishes in time and space. *Environmental Biology of Fishes*, 28(1–4), 33–75.

Cortés, E. (2000). Life history patterns and correlations in sharks. *Reviews in Fisheries Science*, 8: 299-344.

Cowman, P. F., & Bellwood, D. R. (2013). Vicariance across major marine biogeographic barriers: Temporal concordance and the relative intensity of hard versus soft barriers. *Proceedings of the Royal Society B: Biological Sciences*, 280, 20131541.

Cruz, V. M. V., Kilian, A., & Dierig, D. A. (2013). Development of DaRT marker platforms and genetic diversity assessment of the U.S. collection of the new oilseed crop *Lesquerella* and related species. *PLoS ONE*, 8(5), e64062.

Devloo-Delva, F., Burridge, C., Kyne, P., Brunnschweiler, J., Chapman, D., Charvet, P. … Feutry, P. (2023). From rivers to ocean basins: the role of ocean barriers and philopatry in the genetic structuring of a cosmopolitan coastal predator. *Ecology and Evolution*.

Dulvy, N. K., Pacoureau, N., Rigby, C. L., Pollom, R. A., Jabado, R. W., Ebert, D. A., … Simpfendorfer, C. A. (2021). Overfishing drives over one-third of all sharks and rays toward a global extinction crisis. *Current Biology*, 31(21), 4773-4787.

Espinoza, M., Heupel, M. R., Tobin, A. J., & Simpfendorfer, C. A. (2016). Evidence of partial migration in a large coastal predator: opportunistic foraging and reproduction as key drivers? *PLoS ONE*, 11(2), e0147608.

Espinoza, M., Lédée, E. J. I., Smoothey, A. F., Heupel, M. R., Peddemors, V. M., Tobin, A. J., & Simpfendorfer, C. A. (2021). Intra-specific variation in movement and habitat connectivity of a mobile predator revealed by acoustic telemetry and network analyses. *Marine Biology*, 168(6), 1–15.

Excoffier, L., Dupanloup, I., Huerta-Sánchez, E., Sousa, V. C., & Foll, M. (2013). Robust demographic inference from genomic and snp data. *PLoS Genetics*, 9(10), e1003905.

Feldheim, K. A., Gruber, S. H., Dibattista, J. D., Babcock, E. A., Kessel, S. T., Hendry, A. P., … Chapman, D. D. (2014). Two decades of genetic profiling yields first evidence of natal philopatry and long-term fidelity to parturition sites in sharks. *Molecular Ecology*, 23(1), 110–117.

Felsenstein, J. (2006). Accuracy of coalescent likelihood estimates: Do we need more sites, more sequences, or more loci? *Molecular Biology and Evolution*, 23(3), 691–700.

Feutry, P., Berry, O., Kyne, P. M., Pillans, R. D., Hillary, R. M., Grewe, P. M., … Bravington, M. (2017). Inferring contemporary and historical genetic connectivity from juveniles. *Molecular Ecology*, 26(2), 444–456.

Feutry, P., Devloo-Delva, F., Tran Lu Y, A., Mona, S., Gunasekera, R. M., Johnson, G., … Kyne, P. M. (2020). One panel to rule them all: DArTcap genotyping for population structure, historical demography, and kinship analyses, and its application to a threatened shark. *Molecular Ecology Resources*, 20(6), 1470–1485.

Fields A.T., Fischer G.A., Shea S.K.H., Zhang H., Abercrombie D.L., Feldheim K.A., Babcock E.A., Chapman D.D. (2018) Species composition of the international shark fin trade assessed through a retail-market survey in Hong Kong. *Conservation Biology,* 32, 376–389.

Frankham, R., Bradshaw, C. J. A., & Brook, B. W. (2014). Genetics in conservation management: Revised recommendations for the 50/500 rules, Red List criteria and population viability analyses. *Biological Conservation*, 170, 56–63.

Fredston-Hermann A, Gaines SD, Halpern BS. (2018). Biogeographic constraints to marine conservation in a changing climate. *Annals of the New York Academy of Sciences,* 1429, 5–17.

Galván-Quesada, S., Doadrio, I., Alda, F., Perdices, A., Reina, R. G., García Varela, M., ... Domínguez-Domínguez, O. (2016). Molecular phylogeny and biogeography of the amphidromous fish genus Dormitator Gill 1861 (Teleostei: Eleotridae). *PLoS One*, 11(4), e0153538.

Gausmann, P. (2021). Synopsis of global fresh and brackish water occurrences of the bull shark *Carcharhinus leucas* Valenciennes, 1839 (Pisces: Carcharhinidae), with comments on distribution and habitat use. *Integrative Systematics*, 4(1), 55–213.

Gerber, B. D., Ivan, J. S., & Burnham, K. P. (2014). Estimating the abundance of rare and elusive carnivores from photographic-sampling data when the population size is very small. *Population Ecology*, 56(3), 463–470.

Glaus, K. B. J., Appleyard, S. A., Stockwell, B., Brunnschweiler, J. M., Shivji, M. S., Clua, E. G., … Rico, C. (2020). Insights into insular isolation of the bull shark, *Carcharhinus leucas* (Müller and Henle, 1839), in Fijian waters. *Frontiers in Marine Science*, 7, 1–10.

Glaus, K. B. J., Brunnschweiler, J. M., Piovano, S., Mescam, G., Genter, F., Fluekiger, P., & Rico, C. (2019). Essential waters: Young bull sharks in Fiji's largest riverine system. *Ecology and Evolution*, 9(13), 7574–7585.

Gonzalez C, Postaire BD, Domingues RR, Feldheim KA, Caballero S, Chapman DD. (2021). Phylogeography and population genetics of the cryptic bonnethead shark Sphyrna aff. tiburo in Brazil and the Caribbean inferred from mtDNA markers. *Journal of Fish Biology,* 99,1899–1911.

Graham, F., Rynne, P., Estevanez, M., Luo, J., Ault, J. S., & Hammerschlag, N. (2016). Use of marine protected areas and exclusive economic zones in the subtropical western North Atlantic Ocean by large highly mobile sharks. *Diversity and Distributions*, 22(5), 534–546.

Green, A. L., Fernandes, L., Almany, G. R., Abesamis, R., McLeod, E., Aliño, P. M., … Pressey, R. L. (2014). Designing marine reserves for fisheries management, biodiversity conservation, and climate change adaptation. *Coastal Management*, 42(2), 143–159.

Hammerschlag, N., Luo, J., Irschick, D. J., & Ault, J. S. (2012). A comparison of spatial and movement patterns between sympatric predators: bull sharks (*Carcharhinus leucas*) and Atlantic tarpon (*Megalops atlanticus*). *PLoS ONE*, 7(9), e0045958

Harvey, M. G., & Brumfield, R. T. (2015). Genomic variation in a widespread Neotropical bird (*Xenops minutus*) reveals divergence, population expansion, and gene flow. *Molecular Phylogenetics and Evolution*, 83, 305–316.

Heithaus, M. R. (2005). Nursery areas as essential shark habitats. *American Fisheries Society Symposium*, October 1996, 1–12.

Heithaus, M. R., Frid, A., Wirsing, A. J., & Worm, B. (2008). Predicting ecological consequences of marine top predator declines. *Trends in Ecology and Evolution*, 23(4), 202–210.

Heupel, M. R., Simpfendorfer, C. A., Espinoza, M., Smoothey, A. F., Tobin, A. J., & Peddemors, V. (2015). Conservation challenges of sharks with continental scale migrations. *Frontiers in Marine Science*, 2, 1–7.

Hirschfeld, M., Dudgeon, C., Sheaves, M., & Barnett, A. (2021). Barriers in a sea of elasmobranchs: From fishing for populations to testing hypotheses in population genetics. *Global Ecology and Biogeography*, *30*(11), 2147–2163.

Hoarau, F., Darnaude, A., Poirout, T., Jannel, L. A., Labonne, M., & Jaquemet, S. (2021). Age and growth of the bull shark (*Carcharhinus leucas*) around Reunion Island, South West Indian Ocean. *Journal of Fish Biology*, 99(3), 1087–1099.

Hohenlohe, P. A., Funk, W. C., & Rajora, O.P. (2021). Population genomics for wildlife conservation and management. *Molecular Ecology*, 30, 62– 82.

Hou Z, Li S. (2018). Tethyan changes shaped aquatic diversification. *Biological Reviews,* 93, 874–896.

Jombart, T. (2008). Adegenet: A R package for the multivariate analysis of genetic markers. *Bioinformatics*, 24(11), 1403–1405.

Jombart, T., Devillard, S., & Balloux, F. (2010). Discriminant analysis of principal components: A new method for the analysis of genetically structured populations. *BMC Genetics*, 11(1), 94.

Jung, G., Prange, M., & Schulz, M. (2014). Uplift of Africa as a potential cause for Neogene intensification of the Benguela upwelling system. *Nature Geoscience*, 7(10), 741–747.

Karl, S. A., Castro, A. L. F., Lopez, J. A., Charvet, P., & Burgess, G. H. (2011). Phylogeography and conservation of the bull shark (*Carcharhinus leucas*) inferregd from mitochondrial and microsatellite DNA. *Conservation Genetics*, 12(2), 371–382.

Keenan K., Mcinnity P., Cross T. F., Crozier W. W., Prodöhl P. A. (2013). DiveRsity: An R package for the estimation and exploration of population genetics parameters and their associated errors. *Methods in Ecology and Evolution*, 4, 782–788.

Kerdoncuff, E., Lambert, A., & Achaz, G. (2020). Testing for population decline using maximal linkage disequilibrium blocks. *Theoretical Population Biology*, 134, 171–181.

Kottillil S, Rao C, Bowen BW, Shanker K. (2023). Phylogeography of sharks and rays: a global review based on life history traits and biogeographic partitions. *PeerJ* 11:e15396.

Lea, J. S. E., Humphries, N. E., Clarke, C. R., & Sims, D. W. (2015). To Madagascar and back: Long-distance, return migration across open ocean by a pregnant female bull shark *Carcharhinus leucas*. *Journal of Fish Biology*, 87(6), 1313–1321.

Lee, K. A., Smoothey, A. F., Harcourt, R. G., Roughan, M., Butcher, P. A., & Peddemors, V.M (2019). Environmental drivers of abundance and residency of a large migratory shark, Carcharhinus leucas, inshore of a dynamic western boundary current. *Marine Ecology Progress Series*. 622, 121-137.

Lessios, H. A. (2008). The great American schism: Divergence of marine organisms after the rise of the Central american Isthmus. *Annual Review of Ecology, Evolution, and Systematics,* 39, 63–91.

Lesturgie, P., Braun, C. D., Clua, E., Mourier, J., Thorrold, S. R., Vignaud, T., Planes, S., & Mona, S. (2023). Like a rolling stone : Colonization and migration dynamics of the gray reef shark (*Carcharhinus amblyrhynchos*). *Ecology and Evolution*, 13(1), e9746.

Lesturgie, P., Lainé, H., Asuwalski, A., Chifflet-Belle, P., Maisano Delser, P., Magalon, H., & Mona, S. (2022). Life history traits and biogeographic features shaped the complex evolutionary history of an iconic apex predator (*Galeocerdo cuvier*). *BMC Ecology and Evolution*, 22(147), 1–23.

Lesturgie, P., Planes, S., & Mona, S. (2022). Coalescence times, life history traits and conservation concerns: An example from four coastal shark species from the Indo-Pacific. *Molecular Ecology Resources*, 22(2):554-566.

Liu, X., & Fu, Y. X. (2020). Stairway plot 2: Demographic history inference with folded SNP frequency spectra. Genome Biology, 21(1), 1–9

Luikart, G., Ryman, N., Tallmon, D. A., Schwartz, M. K., & Allendorf, F. W. (2010). Estimation of census and effective population sizes: The increasing usefulness of DNA-based approaches. *Conservation Genetics*, 11(2), 355–373.

Maisano Delser, P., Corrigan, S., Duckett, D., Suwalski, A., Veuille, M., Planes, S., … Mona, S. (2019). Demographic inferences after a range expansion can be biased: the test case of the blacktip reef shark (*Carcharhinus melanopterus*). *Heredity*, 122(6), 759–769.

Maisano Delser, P., Corrigan, S., Hale, M., Li, C., Veuille, M., Planes, S., … Mona, S. (2016). Population genomics of *C. melanopterus* using target gene capture data: Demographic inferences and conservation perspectives. *Scientific Reports*, 6, 1–12.

Maisey JG. (2012). What is an "elasmobranch"? The impact of palaeontology in understanding elasmobranch phylogeny and evolution. *Journal of Fish Biology*, (80), 918–951.

Mansfield, B. (2010). "Modern" industrial fisheries and the crisis of overfishing. In *Global political ecology* (pp. 98-113). Routledge.

Matich, P., & Heithaus, M. R. (2012). Effects of an extreme temperature event on the behavior and age structure of an estuarine top predator, *Carcharhinus leucas*. *Marine Ecology Progress Series*, 447, 165–178.

Mazet, O., Rodríguez, W., Grusea, S., Boitard, S., & Chikhi, L. (2016). On the importance of being structured: Instantaneous coalescence rates and human evolution-lessons for ancestral population size inference? *Heredity*, 116(4), 362–371.

Meng, X.-L., & Rubin, D. B. (1993). Maximum likelihood estimation via the ECM algorithm : a general framework. *Biometrika*, 80(2), 267–278.

Momigliano P., Harcourt R., Robbins W.D., Jaiteh V., Mahardika G.N., Sembiring A., Stow A. (2017). Genetic structure and signatures of selection in grey reef sharks (*Carcharhinus amblyrhynchos*). *Heredity*,119, 142–153.

Monteagudo, M. M., Lynch-Stieglitz, J., Marchitto, T. M., & Schmidt, M. W. (2021). Central Equatorial Pacific cooling during the Last Glacial Maximum. *Geophysical Research Letters*, 48(3), 1–10.

Nadachowska-Brzyska, K., Konczal, M., & Babik, W. (2021). Navigating the temporal continuum of effective population size. *Methods in Ecology and Evolution*, 13(1), 22–41.

Niella, Y.; Smoothey, A.F.; Peddemors, V.; Harcourt, R. (2020) Predicting Changes in Distribution of a Large Coastal Shark in the Face of the Strengthening East Australian Current. *Marine Ecology Progress Series*, 642, 163–177.

Nordborg, M. (2019). Coalescent theory. *Handbook of Statistical Genomics*: *Two Volume Set,* 145–30.

Norris, K. E. N. (2004). Managing threatened species: the ecological toolbox, evolutionary theory and declining-population paradigm. *Journal of Applied Ecology*, 41(3), 413-426.

O'Dea, A., Lessios, H. A., Coates, A. G., Eytan, R. I., Restrepo-Moreno, S. A., Cione, A. L, … Jackson, J. B. C. (2016). Formation of the Isthmus of Panama. *Science Advances*, 2(8), 1–12.

Olver, C. H., Shuter, B. J., & Minns, C. K. (1995). Towards a definition of conservation principles for fisheries management. *Canadian Journal of Fisheries and Aquatic Sciences*, 52(7), 1584–1594.

Ouborg, N. J., Pertoldi, C., Loeschcke, V., Bijlsma, R. K., & Hedrick, P. W. (2010). Conservation genetics in transition to conservation genomics. *Trends in Genetics*, 26(4), 177–187.

Pacoureau, N., Rigby, C. L., Kyne, P. M., Sherley, R. B., Winker, H., Carlson, J. K., … Dulvy, N. K. (2021). Half a century of global decline in oceanic sharks and rays. *Nature*, 589(7843), 567–571.

Paris, J. R., Stevens, J. R., & Catchen, J. M. (2017). Lost in parameter space: a road map for stacks. *Methods in Ecology and Evolution*, 8(10), 1360–1373.

Pazmiño, D. A., Maes, G. E., Green, M. E., Simpfendorfer, C. A., Hoyos-Padilla, E. M., Duffy, C. J. A., … Van Herwerden, L. (2018). Strong trans-Pacific break and local conservation units in the Galapagos shark (*Carcharhinus galapagensis*) revealed by genome-wide cytonuclear markers. *Heredity*, 120(5), 407–421.

Peter B.M., Wegmann D., Excoffier L. (2010) Distinguishing between population bottleneck and population subdivision by a Bayesian model choice procedure. *Molecular Ecology*, 19, 4648–4660.

Phillips, N. M., Devloo-Delva, F., McCall, C., & Daly-Engel, T. S. (2021). Reviewing the genetic evidence for sex-biased dispersal in elasmobranchs. *Reviews in Fish Biology and Fisheries*, 31(4), 821–841.

Pirog, A., Jaquemet, S., Ravigné, V., Cliff, G., Clua, E. G., Holmes, B. J., … Magalon, H. (2019). Genetic population structure and demography of an apex predator, the tiger shark *Galeocerdo cuvier*. *Ecology and Evolution*, 9(10), 5551–5571.

Pirog, A., Ravigné, V., Fontaine, M. C., Rieux, A., Gilabert, A., Cliff, G., … Magalon, H. (2019). Population structure, connectivity, and demographic history of an apex marine predator, the bull shark *Carcharhinus leucas*. *Ecology and Evolution*, 9(23), 12980-13000.

Popov S. V., Rögl F., Rozanov A.Y., Steininger F., Shcherba I., Kovac M. (2004) Lithological-paleogeographic maps of Paratethys-10 maps late Eocene to Pliocene. Page (Popov S V., Rögl F, Rozanov AY, Steininger F, Shcherba I, Kovac M, editors) CFS Courier Forschungsinstitut Senckenberg. Frankfurt.

Pudlo, P., Marin, J. M., Estoup, A., Cornuet, J. M., Gautier, M., & Robert, C. P. (2016). Reliable ABC model choice via random forests. *Bioinformatics*, 32(6), 859–866.

R Core Team (2022). R: A language and environment for statistical computing. R Foundation for Statistical Computing, Vienna, Austria.

Raj, A., Stephens, M., & Pritchard, J. K. (2014). fastSTRUCTURE: Variational inference of population structure in large SNP data sets. *Genetics*, 197(2), 573–589.

Raynal, L., Marin, J. M., Pudlo, P., Ribatet, M., Robert, C. P., & Estoup, A. (2019). ABC random forests for Bayesian parameter inference. *Bioinformatics*, 35(10), 1720–1728.

Reed, D. H., & Frankham, R. (2016). Correlation between fitness and genetic diversity. *Conservation Biology*, 17(1), 230–237.

Reid, K., Hoareau, T. B., Graves, J. E., Potts, W. M., Dos Santos, S. M. R., Klopper, A. W., & Bloomer, P. (2016). Secondary contact and asymmetrical gene flow in a cosmopolitan marine fish across the Benguela upwelling zone. *Heredity*, 117(5), 307–315.

Reynolds, J. D., Weir, B. S., & Cockerham, C. C. (1983). Estimation of the coancestry coefficient: Basis for a short-term genetic distance. *Genetics*, 105, 767–779.

Rigby, C. L., Espinoza, M., Derrick, D., Pacoureau, N., & M., D. (2021). *Carcharhinus leucas*. The IUCN Red List of Threatened Species, 2021, e.T39372A2910670.

Robinson, N. M., Scheele, B. C., Legge, S., Southwell, D. M., Carter, O., Lintermans, M., ... & Lindenmayer, D. B. (2018). How to ensure threatened species monitoring leads to threatened species conservation. *Ecological Management & Restoration*, 19(3), 222-229.

Rochette, N. C., Rivera-Colón, A. G., & Catchen, J. M. (2019). Stacks 2: Analytical methods for paired-end sequencing improve RADseq-based population genomics. *Molecular Ecology*, 28(21), 4737–4754.

Roman, J., & Palumbi, S. R. (2003). Whales before whaling in the North Atlantic. *Science*, 301(5632), 508-510.

Rosenberg, N. A. (2004). DISTRUCT: A program for the graphical display of population structure. *Molecular Ecology Notes*, 4(1), 137–138.

Sandoval Laurrabaquio-Alvarado, N., Islas-Villanueva, V., Adams, D. H., Uribe-Alcocer, M., Alvarado-Bremer, J. R., & Díaz-Jaimes, P. (2019). Genetic evidence for regional philopatry of the Bull Shark (*Carcharhinus leucas*), to nursery areas in estuaries of the Gulf of Mexico and western North Atlantic Ocean. *Fisheries Research*, 209, 67–74.

Santiago, E., Novo, I., Pardiñas, A. F., Saura, M., Wang, J., & Caballero, A. (2020). Recent demographic history inferred by high-resolution analysis of linkage disequilibrium. *Molecular Biology and Evolution*, 37(12), 3642–3653.

Smoothey, A. F., Gray, C. A., Kennelly, S. J., Masens, O. J., Peddemors, V. M., & Robinson, W. A. (2016). Patterns of occurrence of sharks in Sydney Harbour, a large urbanised estuary. *PLoS ONE*, 11(1), e0146911.

Smoothey, A. F., Lee, K. A., & Peddemors, V. M. (2019). Long-term patterns of abundance, residency and movements of bull sharks (*Carcharhinus leucas*) in Sydney Harbour, Australia. *Scientific Reports*, 9, 18864.

Smoothey, A. F., Niella, Y., Brand, C., Peddemors, V. M., Butcher, P. A. (2023). Bull Shark (*Carcharhinus leucas*) Occurrence along Beaches of South-Eastern Australia: Understanding Where, When and Why. *Biology*, 12(9), 1189.

Summerhayes, C., & Charman, D. (2015). Introduction to Holocene climate change: new perspectives. *Journal of the Geological Society*, 172(2), 251–253.

Sun, J., Sheykh, M., Ahmadi, N., Cao, M., Zhang, Z., Tian, S., … Talebian, M. (2021). Permanent closure of the Tethyan Seaway in the northwestern Iranian Plateau driven by cyclic sea-level fluctuations in the late Middle Miocene. *Palaeogeography, Palaeoclimatology, Palaeoecology*, 564, 110172.

Tajima, F. (1989). Statistical Method for Testing the Neutral Mutation Hypothesis by DNA Polymorphism. *Genetics*, 123, 585–595.

Teske PR, Von Der Heyden S, McQuaid CD, Barker NP. 2011. A review of marine phylogeography in southern Africa. South African Journal of Science 107:43–53.

Testerman, C. B. (2014). Molecular ecology of globally distributed sharks. Doctoral dissertation. Nova Southeastern University.

Tillett, B. J., Meekan, M. G., Field, I. C., Thorburn, D. C., & Ovenden, J. R. (2012). Evidence for reproductive philopatry in the bull shark *Carcharhinus leucas*. *Journal of Fish Biology*, 80(6), 2140–2158.

Vignaud TM, Mourier J, Maynard JA, Leblois R, Spaet JLY, … Planes S. (2014). Blacktip reef sharks, Carcharhinus melanopterus, have high genetic structure and varying demographic histories in their Indo-Pacific range. *Molecular Ecology,* 23, 5193–5207.

Wakeley, J. (2009). Coaslescent theory : an introduction. Roberts & Co.

Waters, J. M. (2008). Driven by the West Wind Drift? A synthesis of southern temperate marine biogeography, with new directions for dispersalism. *Journal of Biogeography*, 35(3), 417–427.

Watterson, G. A. (1975). On the number of segregating sites in genetical models without recombination. *Theoretical Population Biology*, 276(7), 256–276.

Werry, J. M., Lee, S. Y., Lemckert, C. J., & Otway, N. M. (2012). Natural or artificial? Habitat-use by the bull shark Carcharhinus leucas. PLoSONE, 7(11). https://doi.org/10.1371/journal.pone.0049796

Young, J. L., Bornik, Z. B., Marcotte, M. L., Charlie, K. N., Wagner, G. N., Hinch, S. G., & Cooke, S. J. (2006). Integrating physiology and life history to improve fisheries management and conservation. *Fish and Fisheries*, 7(4), 262–283.

Biosketch

Bautisse Postaire is interested in marine biodiversity and its evolution in response to global changes. He has studied several taxonomic groups in the tropics and worked on the development and application of molecular technologies to describe marine biodiversity and monitor populations' trends.

Author contributions: BDP and FDD contributed equally to this publication, under the guidance of PF and SM. All authors read and approved the manuscript. BDP, FDD, CPB, PF, HM and SM conceived the ideas; all authors collected the data; BDP, FDD, PL and SM analyzed the data; and BDP, FDD, HM, PF and SM led the writing.

Data availability statement

The original 513 FASTQ files (475 individuals) and their metadata, including the final list of 309 individuals used to generate the results of this study. are available on DataDryad (https://doi.org/10.5061/dryad.9zw3r22mn)

Table 1: Summary statistics for each *Carcharhinus leucas* population-specific dataset used in this study, and ABC-RF estimation of the best demographic model. We only reported the estimated parameters values of datasets showing a posterior probability of ≥ 0.5. Prior distributions are set to uniform for all estimated parameters.

Sampling region	*Sampling site*	*Year of sampling*	*Code*	N_{seq}	N_{bio}	N_{loc}	N_{SNP}	*Mean coverage*	*TD*	ϑ_{π}	ϑ_{w}	*Model (prob.)*	N_{mod} *[95% Conf. Int.]*	T_{col} *[95% Conf. Int.]*	N_{anc} *[95% Conf. Int.]*
EPA	Costa Rica	2017-2018	CRI	17	15	5145	695	24.499	-0.75	3.93×10^{-4}	4.87×10^{-4}	SST (0.373)			
WTA	Gulf of Mexico	2011-2017	GOM	47	27	2981	549	27.824	-1.02	4.14×10^{-4}	5.77×10^{-4}	NS (0.973)	16,040 [5,130-37,892]	155,535 [4,216-1,792,297]	4,717 [226-37,537]
WTA	Brazil	2003-2005	BRA	61	40	3408	793	26.347	-1.26	4.28×10^{-4}	6.71×10^{-4}	NS (0.436)			
WTA	U.S. Atlantic coast	1987-2015	NAT	8	7	3569	417	26.954	-0.54	4.63×10^{-4}	5.25×10^{-4}	SST (0.337)			
IPA	South Africa[a]	2009-2015	SAF	28	20	3106	909	28.130	-0.77	7.82×10^{-4}	9.83×10^{-4}	NS (0.594)	17,719 [12,410-39,175]	125,536 [18,558-389,778]	5,334 [170-8,395]
IPA	Arabian/Persian Gulf and Arabian Sea[a]	2010-2012	ARB	23	12	5312	1108	25.114	-0.66	6.68×10^{-4}	7.98×10^{-4}	NS (0.583)	17,454 [8,403-37,213]	99,533 [12,985-304,777]	5,043 [482.33-7,223]
IPA	Seychelles[a]	2013-2016	SEY	36	27	3699	1167	26.266	-1.03	7.09×10^{-4}	9.89×10^{-4}	NS (0.619)	21,084 [12,472-38,888]	110,483 [15,963-304,781]	4,545 [894-7,565]
IPA	Reunion Island[a]	2013-2017	REU	28	20	3095	876	28.084	-0.80	7.49×10^{-4}	9.51×10^{-4}	NS (0.666)	17,071 [12,123-38,887]	130,408 [23,300-332,737]	5,139 [966-8,395]
IPA	Sri Lanka [a]	2017-2018	LKA	12	8	4363	875	26.916	-0.57	7.52×10^{-4}	8.63×10^{-4}	NS (0.502)	22,160.02 [12,152-47,651]	107,423 [16,294-263,978]	5,738 [1,822-8,044]
IPA	Thailand	Not recorded	TAI	6	5	4242	617	26.045	-0.61	6.45×10^{-4}	7.34×10^{-4}	NS (0.124)			
IPA	Darwin	2008	DAR	17	12	4482	949	26.884	-0.60	6.90×10^{-4}	8.10×10^{-4}	NS (0.481)			
IPA	Papua New-Guinea	2018-2019	PNG	12	7	6799	1072	25.470	-0.53	6.26×10^{-4}	7.08×10^{-4}	NS (0.471)			
IPA	Cape York[a]	2002-2009	CAP	27	19	3806	1081	27.302	-0.90	7.35×10^{-4}	9.66×10^{-4}	NS (0.638)	19,887 [12,122-39,175]	110,902 [18,568-304,774]	5,554 [1,332-7,780]
IPA	Sydney[a]	2011-2019	SYD	69	45	3138	1127	28.121	-0.93	7.38×10^{-4}	1.01×10^{-3}	NS (0.620)	16,367 [12,152-29,654]	107,193 [18,668-304,773]	4,912 [1,192-8,216]
IPA	Iriomote Island	2014-2016	IRI	38	29	4210	897	26.668	-0.30	6.02×10^{-4}	6.58×10^{-4}	NS (0.658)	6,727 [5,823-9,026]	1,603,507 [69,952-3,824,732]	18,639 [226-46,643]
IPA	Fiji	2016-2017	FIJ	25	16	2583	558	28.003	-0.40	6.87×10^{-4}	7.66×10^{-4}	NS (0.562)	11,848 [6,854-42,923]	864,559 [12,595-3,730,256]	9,451 [279-44,150]

												Priors	0.5-50,000	13-3,900,000	0.5-50,000

[a] Population used to design the simulation study.

EPA: Eastern Tropical Pacific

WTA: Western Tropical Atlantic

IPA: Western and Central Indo-Pacific

N_{seq}: number of individuals sequenced.

N_{bio}: number of individuals that passed bioinformatic filtering.

N_{loc}: number of loci retained after bioinformatic filtering.

N_{SNP}: number of SNP retained after bioinformatic filtering.

TD: Tajima's D.

θ_{π}: mean pairwise difference.

θ_{W}: Watterson's theta.

N_{mod}: modern N_e expressed in diploid genotypes.

T_{col}: time of the instantaneous change from N_{mod} to N_{anc}, expressed in years before present.

N_{anc}: ancestral N_e expressed in diploid genotypes.

Table 2: Pairwise F_{ST} values. Dotted lines delimit the main biogeographic regions sampled in this study. Values significantly different from 0 after FDR correction (α = 0.05) are in bold.

Sampling site	*CRI*	*GOM*	*BRA*	*NAT*	*SAF*	*ARB*	*SEY*	*REU*	*LKA*	*TAI*	*DAR*	*PNG*	*CAP*	*SYD*	*IRI*
GOM	**0.357**														
BRA	**0.329**	0.005													
NAT	**0.392**	0.010	0.013												
SAF	**0.599**	**0.616**	**0.616**	**0.559**											
ARB	**0.627**	**0.631**	**0.626**	**0.572**	0										
SEY	**0.587**	**0.610**	**0.610**	**0.559**	0	0.002									
REU	**0.599**	**0.617**	**0.617**	**0.559**	0.002	0	0.003								
LKA	**0.656**	**0.646**	**0.638**	**0.591**	0	0	0.001	0.003							
TAI	**0.688**	**0.656**	**0.645**	**0.609**	0	0	0.007	0.001	0.005						
DAR	**0.619**	**0.625**	**0.621**	**0.563**	0	0.002	0	0.003	0.006	0.004					
PNG	**0.663**	**0.650**	**0.641**	**0.596**	0	0.001	0.003	0.005	0	0.011	0.005				
CAP	**0.605**	**0.622**	**0.621**	**0.566**	0.005	0.004	0.007	0.005	0.003	0.006	0.005	0.006			
SYD	**0.558**	**0.587**	**0.589**	**0.541**	0	0	0	0.002	0	0.004	0	0	0.003		
IRI	**0.602**	**0.623**	**0.623**	**0.577**	**0.047**	**0.046**	**0.040**	**0.042**	**0.049**	**0.050**	**0.044**	**0.044**	**0.040**	**0.038**	
FIJ	**0.629**	**0.635**	**0.631**	**0.585**	**0.032**	**0.026**	**0.032**	**0.033**	**0.032**	**0.037**	**0.040**	0.028	**0.033**	**0.031**	**0.075**

Table 3 : Summary statistics averaged over 10 replicates of coalescent simulations of 5,000 loci (100 bp each) under the NS and NS_{BOT} models with a mutation rate of 2.509×10^{-8} per site per generation.

T_{BOT}	*BOT*	*TD*	ϑ_π	ϑ_w	*S*
-	-	-0.89	6.9×10^{-4}	8.9×10^{-4}	1760.4
5	5	-0.86	7.0×10^{-4}	9.0×10^{-4}	1773.6
	10	-0.87	6.8×10^{-4}	8.8×10^{-4}	1734
	50	-0.80	6.8×10^{-4}	8.6×10^{-4}	1701.3
	100	-0.67	6.8×10^{-4}	8.2×10^{-4}	1623.4
50	5	-0.81	6.8×10^{-4}	8.5×10^{-4}	1688.2
	10	-0.69	6.8×10^{-4}	8.3×10^{-4}	1635.8
	50	-0.10	6.4×10^{-4}	6.6×10^{-4}	1306.6
	100	0.43	5.9×10^{-4}	5.3×10^{-4}	1056.1
450	5	-0.31	6.6×10^{-4}	7.2×10^{-4}	1426.8
	10	0.14	6.2×10^{-4}	6.0×10^{-4}	1183.6
	50	1.27	3.6×10^{-4}	2.7×10^{-4}	543
	100	1.32	1.9×10^{-4}	1.4×10^{-4}	282
1500	5	0.24	5.9×10^{-4}	5.6×10^{-4}	1109.6
	10	0.72	4.7×10^{-4}	3.9×10^{-4}	781.5
	50	0.86	1.0×10^{-4}	8.1×10^{-5}	160
	100	0.43	2.5×10^{-5}	2.2×10^{-5}	43.5

T_{BOT}: onset of the bottleneck in number of generations
BOT: reduction factor applied to N_{mod}
θ_π: mean pairwise difference
θ_w: Watterson's theta
TD: Tajima's D
S: number of segregating sites

Table 4: Parameter estimation using *fastsimcoal* under the most likely divergence model. Composite maximum likelihood estimates of effective population sizes are presented in number of (diploid) individuals per population, divergence times in number of years (generation time = 13 years), and migration rates are expressed as number of migrants per generation (*Nm*, backward in time). One hundred parametric bootstrap replicates were used to calculate the 95% confidence intervals.

Parameters	*Initial boundaries*	*Estimated value [95% confidence interval]*
N_e1 : WTA modern *Ne*	0.5 - 50,000	3,486 [1,637-4,397]
N_e2 : EPA modern *Ne*	0.5 - 50,000	7,284.5 [5,020-7,179]
N_e3 : IPA modern *Ne*	0.5 - 50,000	14,484 [9,928-10,681]
T_1 : divergence time between WTA and EPA	130 - 1,300,000	40,937 [36,626-76,837]
$N_{anc}2$: WTA - EPA ancestral *Ne*	0.5 - 50,000	135 [118-1,726]
T_2: divergence between WTA-EPA and IPA	130 - 1,300,000	56,121 [173,725-261,880]
$N_{anc}1$: WTA – EPA - IPA ancestral *Ne*	0.5 - 50,000	218 [126-2,997]
Migration rate from WTA to EPA	1 x 10^{-7} - 0.01	0.31 [0.0020-1.61]
Migration rate from EPA to WTA	1 x 10^{-7} - 0.01	0.026 [0.013-0.50]
Migration rate from WTA to IPA	1 x 10^{-7} - 0.01	0.13 [0.042-0.36]
Migration rate from IPA to WTA	1 x 10^{-7} - 0.01	0.019 [0.0014-0.011]
Migration rate from IPA to EPA	1 x 10^{-7} - 0.01	0.0032 [0.0018-0.015]
Migration rate from EPA to IPA	1 x 10^{-7} - 0.01	0.059 [0.034-0.11]

EPA: Eastern Tropical Pacific
WTA: Western Tropical Atlantic
IPA: Western and Central Indo-Pacific

[double column] Figure 1: Distribution range (blue) and sampling locations (orange) of *Carcharhinus leucas populations.* In parentheses, the number of individuals sequenced (left) and the number of individuals that passed bioinformatic filtering (right). CRI: Costa Rica, GOM: Gulf of Mexico, BRA: Brazil, NAT: U.S. Atlantic coast, SAF: South Africa, ARB: Arabian/Persian Gulf and Arabian Sea, SEY: Seychelles, REU: Reunion Island, LKA: Sri Lanka, TAI: Thailand, DAR: Darwin, PNG: Papua New Guinea, CAP: Cap York, SYD: Sydney, IRI: Iriomote Island, FIJ: Fiji. Distribution range is based on IUCN SSC Shark Specialist Group 2020. *Carcharhinus leucas. The IUCN Red List of Threatened Species. Version 2022-2*. https://www.iucnredlist.org. Downloaded on 20 May 2023.

[double column] Figure 2: Population tree topologies of the four scenarios relating to the three genetic clusters identified in this study. N_e: modern effective population size, N_{anc}: ancestral effective population size, T_1: first time of divergence; T_2: second time of divergence; EPA: Eastern Tropical Pacific; IPA: Western and Central Indo-Pacific; WTA: Western Tropical Atlantic.

[double column] Figure 3: Variations of the median effective population size (N_e) through time and its 75% confidence interval estimated by STAIRWAYPLOT. The grey area indicates the last glacial period. a) Western Tropical Atlantic; b) Eastern Tropical Pacific; c) Indo-West Pacific; d) Central Indo-Pacific.

[double column] Figure 4: STAIRWAYPLOT estimates averaged over 10 replicates of the effective population size (N_e) variations through time of scenarios: a) NS; b) NS_{BOT} with a bottleneck starting 5 generations ago with intensity BOT=5; c) BOT=10; d) BOT=50; and e) BOT=100. The median values are presented in bold and their 75% confidence intervals as shaded areas. All scenarios are based on coalescent simulations of 5,000 loci (100 bp each) with a mutation rate of 2.509×10^{-8} per site per generation of 5 (red), 10 (green), 15 (blue) and 20 (purple) diploid individuals. The grey dotted line represents the true (simulated) N_e variation through time.

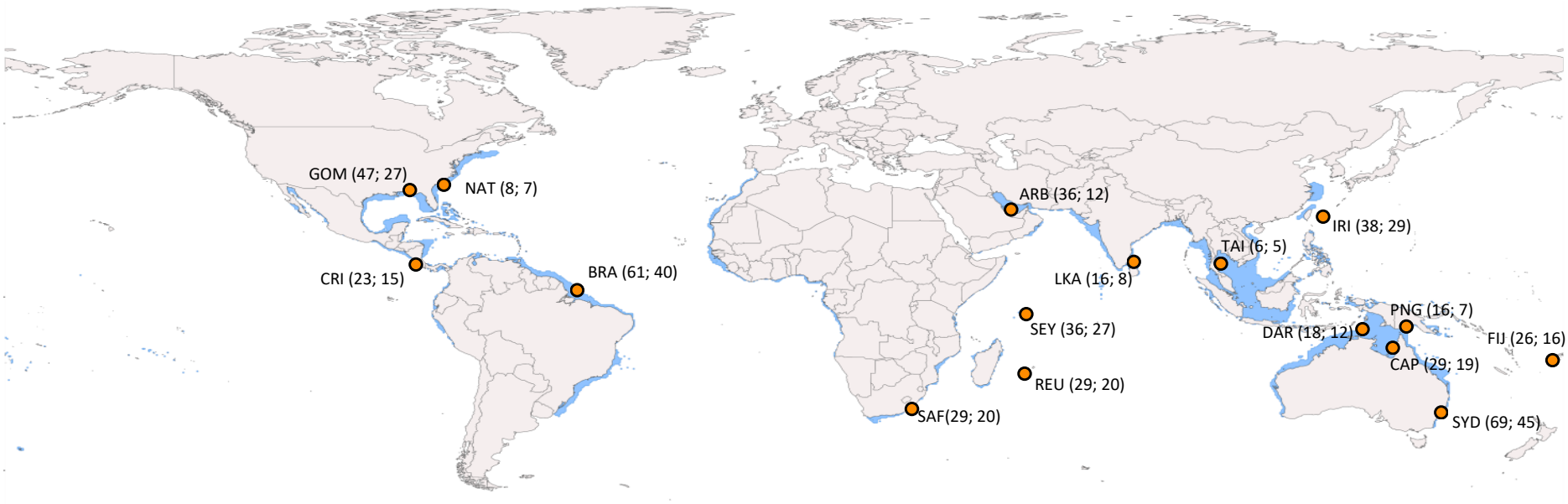
GOM (47; 27)
NAT (8; 7)
CRI (23; 15)
BRA (61; 40)
ARB (36; 12)
LKA (16; 8)
SEY (36; 27)
REU (29; 20)
SAF(29; 20)
IRI (38; 29)
TAI (6; 5)
PNG (16; 7)
DAR (18; 12)
CAP (29; 19)
FIJ (26; 16)
SYD (69; 45)

Figure 1

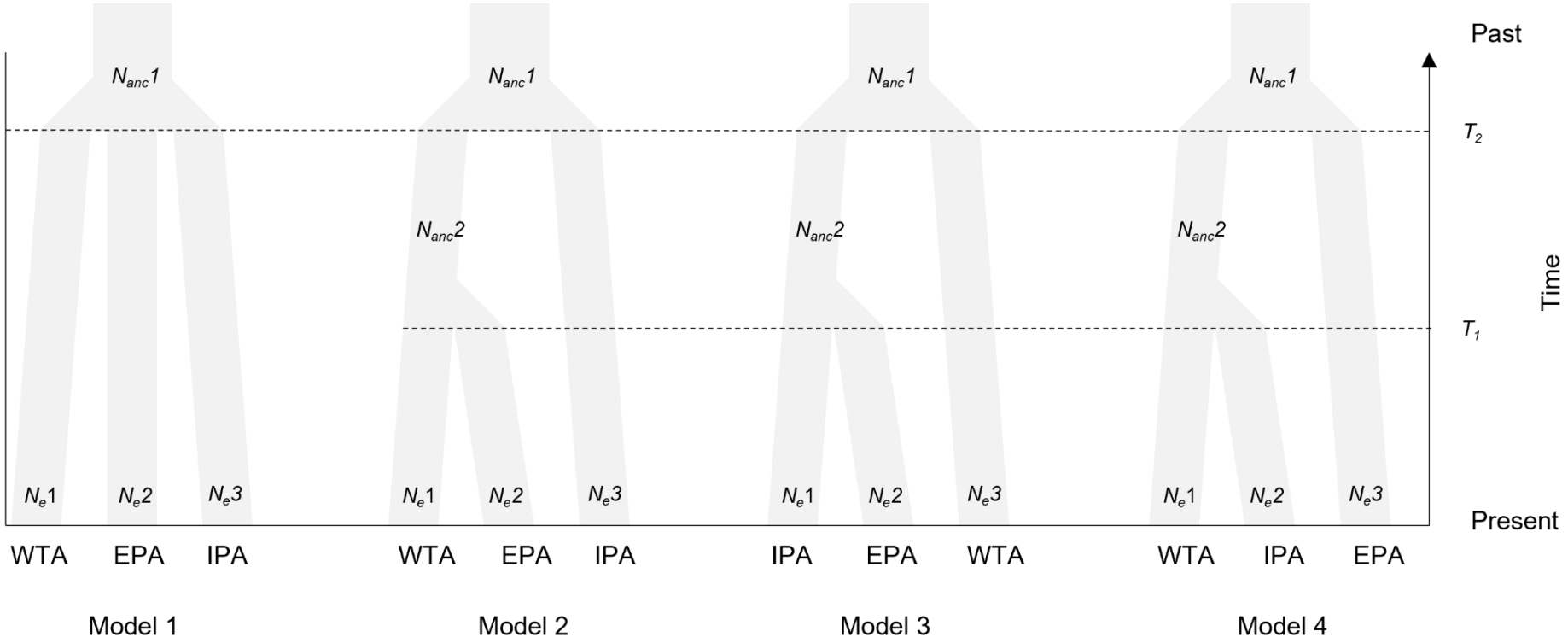
Past
$N_{anc}1$
T_2
$N_{anc}2$
Time
T_1
N_e1
N_e2
N_e3
Present
WTA
EPA
IPA
Model 1
Model 2
Model 3
Model 4

Figure 2

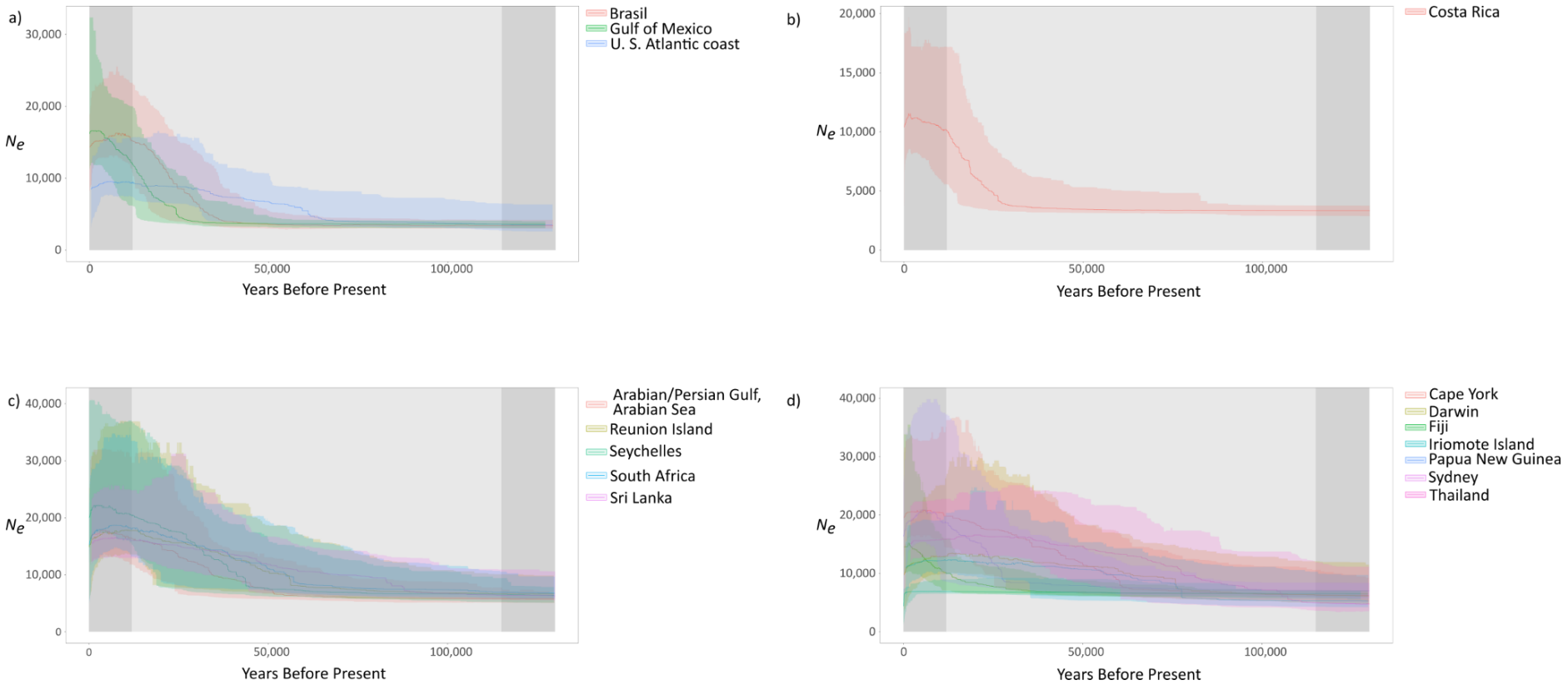
a)
30,000
20,000
N_e
10,000
0
0
50,000
100,000
Years Before Present
Brasil
Gulf of Mexico
U. S. Atlantic coast
b)
20,000
15,000
N_e 10,000
5,000
0
0
50,000
100,000
Years Before Present
Costa Rica
c)
40,000
30,000
N_e 20,000
10,000
0
0
50,000
100,000
Years Before Present
Arabian/Persian Gulf, Arabian Sea
Reunion Island
Seychelles
South Africa
Sri Lanka
d)
40,000
30,000
N_e 20,000
10,000
0
0
50,000
100,000
Years Before Present
Cape York
Darwin
Fiji
Iriomote Island
Papua New Guinea
Sydney
Thailand

Figure 3

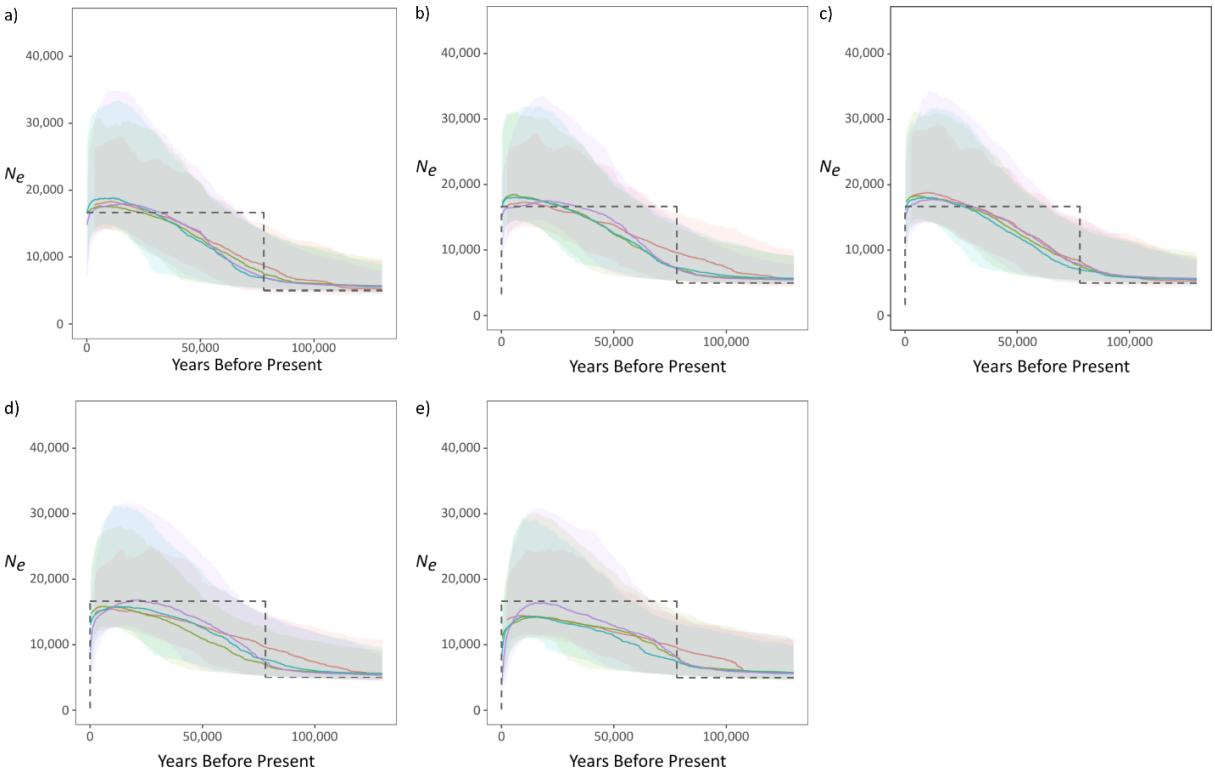
a)
b)
c)
d)
e)
N_e
40,000
30,000
20,000
10,000
0
0
50,000
100,000
Years Before Present

Figure 4

Supplementary Material 1 :

Carcharhinus leucas samples sequenced with the DArTcap panel developped for this study and their associated metadata when available. N_{seq} : Number of individuals sampled and sequenced; N_{bait} : number of samples used for bait design; N_{bio} : number of individuals that passed bioinformatic filtering; Nb_{male} : number of males analysed; Nb_{female} : number of females analysed; $Nb_{unknown}$:

Sampling site	*Sampling year*	N_{bai}	N_{seq}	N_{bio}	Nb_{male}
Australia	*2002-2019*	*47*	-	-	-
Arabian Sea	*2010-2012*	11	23	12	5
Brazil	2003-2005	12	61	40	-
Cape York (Australia)	*2002-2009*	-	27	19	6
Caribbean Sea	*1985-2012*	2	2	-	-
Costa Rica	*2017-2018*	9	17	15	13
Darwin coastal (Australia)	*2008*	-	17	12	7
Fiji	*2016-2017*	11	25	16	2
Gulf of Mexico	*2011-2017*	11	47	27	15
Indonesia	*2002-2019*	6	6	-	-
Iriomote Island	*2014-2016*	12	38	29	14
Mozambique	*2012-2013*	8	12	-	-
Papua New Guinea	*2018-2019*	6	12	7	-
Reunion Island	*2013-2017*	9	28	20	11
Seychelles	*2013-2016*	10	36	27	3
Sierra Leone	*2006*	1	1	-	-
South Africa	*2009-2015*	9	28	20	12
Sri Lanka	*2017-2018*	9	12	8	3
Sydney (Australia)	*2011-2019*	-	69	45	28
Thailand	*Not recorded*	7	6	5	-
U.S. Atlantic coast	*1987-2015*	8	8	7	1

Nb_{female}	Nb_{unkown}	F_{IS}
-	-	-
7	-	0.002
-	40	0.010
3	10	-0.001
-	-	-
2	-	-0.035
5	-	-0.005
14	-	0.048
12	-	-0.013
-	-	-
15	-	-0.063
-	-	-
-	7	-0.018
9	-	0.021
24	-	-0.001
-	-	-
7	1	0.016
4	1	-0.020
17	-	0.016
-	5	-0.027
6	-	0.009

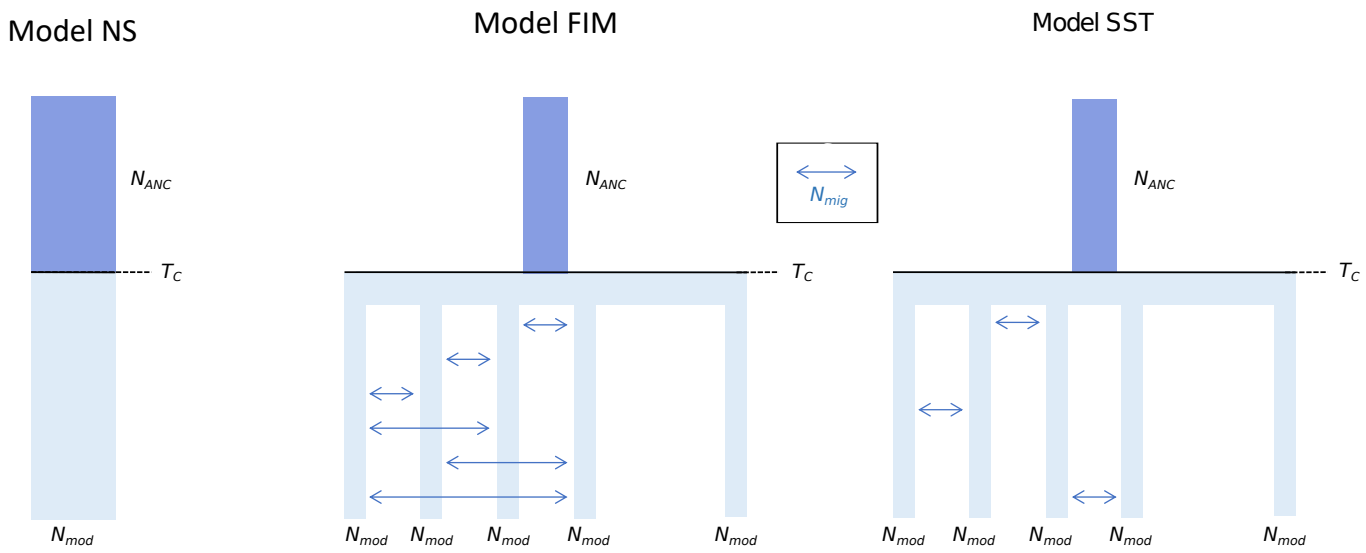

Supplementary material 2: Demographic scenarios investigated in each sampling site with N > 5 individuals by means of an ABC-RF framework coupled to coalescent simulations. N_{mod}: modern effective population size; N_{anc}: ancestral effective population size; N_{mig}: total number of migrants per generation; T_c: time of switch between N_{mod} and N_{anc}.

Supplementary material 3

Demographic scenarios simulated with *fastimcoal* under the NS model, to which an instantaneous bottleneck was added at T_{BOT} generations before present with an intensity *BOT* (defined as the ratio between the *Ne* before and after the bottleneck). The demographic trajectory before the bottleneck is an NS model with an instantaneous expansion, with parameters fixed to the average values estimated in the real data with the STAIRWAYPLOT (see the main text). The mutation rate was fixed to 2.509×10^{-8} per site per generation as in the analyses of real data. The summary statistics represent the average values computed over 10 simulations of dataset of the same size. N_{loc}: number of simulated independent loci (100 bp each), N_{samp}: number of simulated diploid individuals; T_{BOT} : onset of the bottleneck (in generations before present), BOT: strength of the bottleneck, TD: Tajima's D, θ_{π} : Tajima's estimator; θ_{s} : Watterson's estimator; S: number of segregating sites.

N_{loc}	N_{samp}	T_{BOT}	BOT	TD	
	1000	5	0	0	-0.573571165
	1000	10	0	0	-0.80284103
	1000	15	0	0	-0.885019787
	1000	20	0	0	-0.958183565
	5000	5	0	0	-0.549780444
	5000	10	0	0	-0.730080761
	5000	15	0	0	-0.888874705
	5000	20	0	0	-0.91919916
	10000	5	0	0	-0.521722325
	10000	10	0	0	-0.756587302
	10000	15	0	0	-0.905918101
	10000	20	0	0	-0.949478437
	1000	5	5	5	-0.482211748
	1000	10	5	5	-0.749489729
	1000	15	5	5	-0.819563763
	1000	20	5	5	-0.913344225
	5000	5	5	5	-0.530695419
	5000	10	5	5	-0.749022488
	5000	15	5	5	-0.858253168
	5000	20	5	5	-0.909888609
	10000	5	5	5	-0.509056983
	10000	10	5	5	-0.757747507
	10000	15	5	5	-0.870008552
	10000	20	5	5	-0.964389508
	1000	5	5	10	-0.536278097
	1000	10	5	10	-0.737033799
	1000	15	5	10	-0.90572574
	1000	20	5	10	-0.902771285
	5000	5	5	10	-0.546625136
	5000	10	5	10	-0.744375103
	5000	15	5	10	-0.868257378
	5000	20	5	10	-0.916465506
	10000	5	5	10	-0.513886555
	10000	10	5	10	-0.741017079
	10000	15	5	10	-0.863598594
	10000	20	5	10	-0.926509247
	1000	5	5	50	-0.47789151
	1000	10	5	50	-0.660213659
	1000	15	5	50	-0.795671878
	1000	20	5	50	-0.827625964
	5000	5	5	50	-0.495500363
	5000	10	5	50	-0.659678049
	5000	15	5	50	-0.804904846
	5000	20	5	50	-0.832653589
	10000	5	5	50	-0.486803181
	10000	10	5	50	-0.653793059

10000	15	5	50	-0.791670784
10000	20	5	50	-0.847385173
1000	5	5	100	-0.452817019
1000	10	5	100	-0.591630728
1000	15	5	100	-0.604295043
1000	20	5	100	-0.727154904
5000	5	5	100	-0.447272344
5000	10	5	100	-0.631082781
5000	15	5	100	-0.672027368
5000	20	5	100	-0.665309537
10000	5	5	100	-0.416360082
10000	10	5	100	-0.626892727
10000	15	5	100	-0.68360942
10000	20	5	100	-0.717439514
1000	5	50	5	-0.524978679
1000	10	50	5	-0.699651329
1000	15	50	5	-0.743867172
1000	20	50	5	-0.80000877
5000	5	50	5	-0.51203336
5000	10	50	5	-0.679122623
5000	15	50	5	-0.812717298
5000	20	50	5	-0.866160824
10000	5	50	5	-0.481429671
10000	10	50	5	-0.698610829
10000	15	50	5	-0.797007591
10000	20	50	5	-0.852949766
1000	5	50	10	-0.459214808
1000	10	50	10	-0.649396761
1000	15	50	10	-0.670511307
1000	20	50	10	-0.731849053
5000	5	50	10	-0.434254847
5000	10	50	10	-0.625333813
5000	15	50	10	-0.685309127
5000	20	50	10	-0.724400726
10000	5	50	10	-0.414365158
10000	10	50	10	-0.620557894
10000	15	50	10	-0.700771331
10000	20	50	10	-0.747062711
1000	5	50	50	-0.200656283
1000	10	50	50	-0.205093064
1000	15	50	50	-0.09054668
1000	20	50	50	-0.000937262
5000	5	50	50	-0.133163452
5000	10	50	50	-0.120003301
5000	15	50	50	-0.10492077
5000	20	50	50	-0.034248119
10000	5	50	50	-0.152454494

10000	10	50	50	-0.138572921
10000	15	50	50	-0.089772984
10000	20	50	50	-0.04495082
1000	5	50	100	0.098728212
1000	10	50	100	0.266261394
1000	15	50	100	0.434199401
1000	20	50	100	0.472383665
5000	5	50	100	0.158072834
5000	10	50	100	0.285883814
5000	15	50	100	0.432675099
5000	20	50	100	0.531011008
10000	5	50	100	0.116646455
10000	10	50	100	0.253872959
10000	15	50	100	0.429284493
10000	20	50	100	0.513248495
1000	5	450	5	-0.256678447
1000	10	450	5	-0.252801718
1000	15	450	5	-0.389488437
1000	20	450	5	-0.392974377
5000	5	450	5	-0.238143671
5000	10	450	5	-0.327895309
5000	15	450	5	-0.30985484
5000	20	450	5	-0.338676264
10000	5	450	5	-0.251392896
10000	10	450	5	-0.327546766
10000	15	450	5	-0.332178774
10000	20	450	5	-0.319152042
1000	5	450	10	-0.017021052
1000	10	450	10	0.085847883
1000	15	450	10	0.240283096
1000	20	450	10	0.282847507
5000	5	450	10	-0.012560222
5000	10	450	10	0.066839472
5000	15	450	10	0.138781226
5000	20	450	10	0.253057859
10000	5	450	10	-0.005951439
10000	10	450	10	0.062917277
10000	15	450	10	0.123806198
10000	20	450	10	0.230429877
1000	5	450	50	0.759247603
1000	10	450	50	1.103149328
1000	15	450	50	1.226779513
1000	20	450	50	1.534375774
5000	5	450	50	0.645593948
5000	10	450	50	1.088409296
5000	15	450	50	1.270952401
5000	20	450	50	1.510303701

10000	5	450	50	0.625022206
10000	10	450	50	1.092953226
10000	15	450	50	1.307922343
10000	20	450	50	1.538233903
1000	5	450	100	0.654683431
1000	10	450	100	1.127669581
1000	15	450	100	1.474561793
1000	20	450	100	1.526266505
5000	5	450	100	0.796417724
5000	10	450	100	1.062255318
5000	15	450	100	1.323728767
5000	20	450	100	1.574253442
10000	5	450	100	0.655443832
10000	10	450	100	1.183124289
10000	15	450	100	1.442074872
10000	20	450	100	1.552827365
1000	5	1500	5	0.035239145
1000	10	1500	5	0.112502395
1000	15	1500	5	0.202887285
1000	20	1500	5	0.283222128
5000	5	1500	5	0.061258096
5000	10	1500	5	0.149613563
5000	15	1500	5	0.238267922
5000	20	1500	5	0.239392152
10000	5	1500	5	0.061523282
10000	10	1500	5	0.158366636
10000	15	1500	5	0.194614705
10000	20	1500	5	0.253634814
1000	5	1500	10	0.31999144
1000	10	1500	10	0.660079468
1000	15	1500	10	0.807377864
1000	20	1500	10	0.795572813
5000	5	1500	10	0.365063747
5000	10	1500	10	0.615848826
5000	15	1500	10	0.721896674
5000	20	1500	10	0.826339161
10000	5	1500	10	0.410286824
10000	10	1500	10	0.593908443
10000	15	1500	10	0.753218038
10000	20	1500	10	0.860277316
1000	5	1500	50	0.485668371
1000	10	1500	50	0.625059933
1000	15	1500	50	0.806947743
1000	20	1500	50	0.891323387
5000	5	1500	50	0.451412506
5000	10	1500	50	0.74246035
5000	15	1500	50	0.857522794

5000	20	1500	50	0.988074937
10000	5	1500	50	0.410988465
10000	10	1500	50	0.736907824
10000	15	1500	50	0.860905171
10000	20	1500	50	1.008810842
1000	5	1500	100	0.381325713
1000	10	1500	100	-0.239838258
1000	15	1500	100	-0.031398329
1000	20	1500	100	0.285009654
5000	5	1500	100	0.110700141
5000	10	1500	100	0.438159074
5000	15	1500	100	0.432752045
5000	20	1500	100	0.319263869
10000	5	1500	100	0.115661608
10000	10	1500	100	0.30922601
10000	15	1500	100	0.46700355
10000	20	1500	100	0.52687333

θ_π	θ_w	S
0.0006738	0.000761055	215.3
0.000693574	0.000859139	304.8
0.000688214	0.000891042	353
0.000689624	0.000927227	394.4
0.000684862	0.000768973	1087.7
0.000701236	0.000849442	1506.8
0.000686877	0.00088872	1760.4
0.000702198	0.000929249	1976.3
0.000696493	0.000777244	2198.8
0.000695058	0.000847977	3008.4
0.000684499	0.000890436	3527.6
0.000694799	0.000929037	3951.7
0.0007018	0.000777669	220
0.000689437	0.000840535	298.2
0.000703014	0.000891042	353
0.000719565	0.000952853	405.3
0.000696542	0.000778941	1101.8
0.000692265	0.000842847	1495.1
0.000698974	0.000895384	1773.6
0.00070201	0.000925863	1969.1
0.000688913	0.00076664	2168.8
0.000689067	0.000840986	2983.6
0.000695271	0.000893743	3540.7
0.000686767	0.000923066	3926.3
0.000677667	0.000759287	214.8
0.000698805	0.000848428	301
0.00066692	0.000869334	344.4
0.0006912	0.000911475	387.7
0.000688311	0.000772437	1092.6
0.000703052	0.000854967	1516.6
0.000681331	0.000875392	1734
0.000707217	0.000934938	1988.4
0.000696196	0.000775583	2194.1
0.000689022	0.000836899	2969.1
0.0006933	0.000889326	3523.2
0.000692392	0.000918387	3906.4
0.0006584	0.000728181	206
0.000687095	0.000816013	289.5
0.000680218	0.000853431	338.1
0.000703526	0.000903952	384.5
0.000688222	0.000763529	1080
0.000682675	0.000810262	1437.3
0.000682537	0.000858884	1701.3
0.000684161	0.000878562	1868.5
0.000678949	0.000751864	2127
0.000704296	0.000834306	2959.9

0.000692132	0.000867239	3435.7
0.000685015	0.000883898	3759.7
0.000694911	0.000764236	216.2
0.000689553	0.000804174	285.3
0.000692671	0.000819607	324.7
0.000698328	0.000866337	368.5
0.00069292	0.000760843	1076.2
0.000680318	0.000801017	1420.9
0.000678952	0.000819557	1623.4
0.000692121	0.000840805	1788.2
0.000679844	0.000741436	2097.5
0.000677257	0.000796282	2825
0.000684874	0.000829628	3286.7
0.000676274	0.000835421	3553.5
0.000695711	0.000776962	219.8
0.000700453	0.000841381	298.5
0.000688595	0.000851665	337.4
0.000697486	0.000887966	377.7
0.00068128	0.000758722	1073.2
0.000690778	0.000824356	1462.3
0.000675271	0.00085227	1688.2
0.000686011	0.000891163	1895.3
0.00068966	0.000762822	2158
0.000691804	0.000830162	2945.2
0.000691584	0.000868122	3439.2
0.000683002	0.000882982	3755.8
0.000711956	0.000783678	221.7
0.000699163	0.00082926	294.2
0.000675306	0.000815821	323.2
0.000678896	0.000843532	358.8
0.000678116	0.00074232	1050
0.000691628	0.000812799	1441.8
0.000681303	0.000825817	1635.8
0.000681441	0.000844002	1795
0.000685898	0.000747587	2114.9
0.000686694	0.000805978	2859.4
0.000680803	0.000828997	3284.2
0.000679903	0.00084814	3607.6
0.000672	0.000699548	197.9
0.000625458	0.000658166	233.5
0.000638149	0.000653515	258.9
0.000620695	0.000620659	264
0.0006428	0.000660382	934.1
0.000657221	0.000676656	1200.3
0.000641878	0.000659624	1306.6
0.000646589	0.000652585	1387.9
0.00064748	0.00066777	1889.1

0.000644557	0.000666593	2364.9
0.000653342	0.00066866	2649
0.000638455	0.000646097	2748.2
0.000618378	0.000607289	171.8
0.000595789	0.000559793	198.6
0.000624828	0.000561634	222.5
0.0005933	0.000526385	223.9
0.000603267	0.000584807	827.2
0.000597926	0.000559737	992.9
0.000592058	0.000533161	1056.1
0.000592729	0.000519285	1104.4
0.000601498	0.000587811	1662.9
0.000582531	0.000549251	1948.6
0.000593335	0.000534701	2118.3
0.00059296	0.000521777	2219.4
0.000658089	0.000693539	196.2
0.000669947	0.00071313	253
0.000631251	0.000701475	277.9
0.000650109	0.000725983	308.8
0.000658427	0.000691135	977.6
0.000663384	0.000719557	1276.4
0.000663263	0.000720305	1426.8
0.000653244	0.000717896	1526.8
0.000657022	0.000691666	1956.7
0.000657509	0.000713299	2530.6
0.0006573	0.00071816	2845.1
0.000651253	0.000711619	3026.9
0.000621689	0.000624256	176.6
0.000621253	0.000608556	215.9
0.000627283	0.000590662	234
0.000633679	0.000588686	250.4
0.000619524	0.000621004	878.4
0.000619057	0.000609346	1080.9
0.000618763	0.000597528	1183.6
0.000627479	0.000587698	1249.9
0.000619393	0.00062012	1754.3
0.000615799	0.000606668	2152.3
0.000607654	0.000589097	2333.8
0.000615201	0.000579752	2466
0.000387667	0.000335458	94.9
0.000346453	0.000273132	96.9
0.000362147	0.00027438	108.7
0.00037104	0.000261899	111.4
0.000366613	0.000324712	459.3
0.000354801	0.000281531	499.4
0.000363333	0.000274128	543
0.000365144	0.000260301	553.6

0.000363442	0.000323227	914.4
0.000364027	0.000288719	1024.3
0.000361882	0.000271124	1074.1
0.000366307	0.000259948	1105.7
0.000187578	0.000165078	46.7
0.000183232	0.00014319	50.8
0.000204943	0.000147666	58.5
0.000184767	0.000130009	55.3
0.000192467	0.000165997	234.8
0.000186132	0.000148376	263.2
0.000190942	0.000142365	282
0.000183511	0.000128975	274.3
0.000186733	0.000165113	467.1
0.000190683	0.000148658	527.4
0.000190699	0.000139235	551.6
0.00018585	0.000131443	559.1
0.000594422	0.000590675	167.1
0.000590916	0.000575014	204
0.000589908	0.000560372	222
0.000577296	0.000535318	227.7
0.00058816	0.00058106	821.9
0.000587746	0.000567516	1006.7
0.000594341	0.00056017	1109.6
0.000582398	0.000547261	1163.9
0.000583922	0.000576853	1631.9
0.000581377	0.000560272	1987.7
0.000588023	0.000560221	2219.4
0.000591459	0.000554126	2357
0.000465356	0.000436201	123.4
0.000505205	0.000436052	154.7
0.000488703	0.000404629	160.3
0.000465354	0.000382975	162.9
0.000469498	0.000437686	619.1
0.000486651	0.000424101	752.3
0.000467323	0.000394532	781.5
0.000480115	0.00039346	836.8
0.000487911	0.000451083	1276.1
0.000478757	0.000419366	1487.8
0.000467873	0.000392361	1554.4
0.000472813	0.000384832	1636.9
0.000106111	9.69E-05	27.4
9.31E-05	8.06E-05	28.6
9.34E-05	7.70E-05	30.5
9.01E-05	7.19E-05	30.6
0.000100729	9.23E-05	130.6
0.000103086	8.75E-05	155.2
9.88E-05	8.08E-05	160

9.38E-05	7.40E-05	157.3
9.85E-05	9.10E-05	257.3
9.50E-05	8.07E-05	286.3
9.50E-05	7.78E-05	308.4
9.86E-05	7.77E-05	330.4
2.54E-05	2.30E-05	6.5
2.12E-05	2.25E-05	8
2.33E-05	2.40E-05	9.5
2.31E-05	2.12E-05	9
2.56E-05	2.49E-05	35.2
2.59E-05	2.32E-05	41.2
2.45E-05	2.20E-05	43.5
2.19E-05	2.01E-05	42.8
2.36E-05	2.30E-05	65.1
2.31E-05	2.15E-05	76.3
2.58E-05	2.29E-05	90.9
2.70E-05	2.36E-05	100.5

Supplementary Material 4

Model selection analyses performed with *fastsimcoal* . Topology number corresponds to the population trees presented in Figure 2. Secondary contact between EPA and WTA started 8 generations before present corresponding to 100 years ago, which is the approximate date of opening of the Panama Canal. The AIC score is computed as explained in the main text, the lower values representing the most likely scenario. EPA: Eastern Tropical Pacific , WTA: Western Tropical Atlantic, IPA: Western and Central Indo-Pacific

Topology	*Oldest diverging genetic cluster*	*Migration*
Model 2	IPA	Yes
Model 2	IPA	Yes
Model 2	IPA	No
Model 2	IPA	No
Model 2	IPA	No
Model 2	IPA	No
Model 2	IPA	No
Model 3	WTA	No
Model 4	EPA	No
Model 1	NA	No
Model 4	EPA	No
Model 1	NA	No
Model 3	WTA	No
Model 1	NA	No
Model 1	NA	No
Model 4	EPA	No
Model 4	EPA	No
Model 3	WTA	No
Model 3	WTA	No
Model 1	NA	No
Model 4	EPA	No
Model 3	WTA	No

Migration rates	*Secondary contact between EPA and WTA*
6	No
3	No
-	No
-	Yes starting 8 generations ago
-	Yes starting 8 generations ago
-	Yes
-	Yes
-	Yes
-	Yes
-	Yes
-	Yes
-	Yes
-	Yes
-	Yes starting 8 generations ago
-	Yes starting 8 generations ago
-	Yes starting 8 generations ago
-	Yes starting 8 generations ago
-	Yes starting 8 generations ago
-	Yes starting 8 generations ago
-	No
-	No
-	No

Secondary contact migration rates	*AIC score*
-	36832.28391
-	36855.37016
-	36928.31199
1	36931.69815
2	36933.27907
1	36934.10801
2	36935.98827
2	37012.16239
2	37012.17621
2	37043.75575
1	37076.62881
1	37080.93193
1	37081.62542
1	37094.00466
2	37096.4928
1	37096.96849
2	37099.13888
1	37100.13224
2	37102.74473
-	37115.83641
-	37122.22189
-	37122.41531

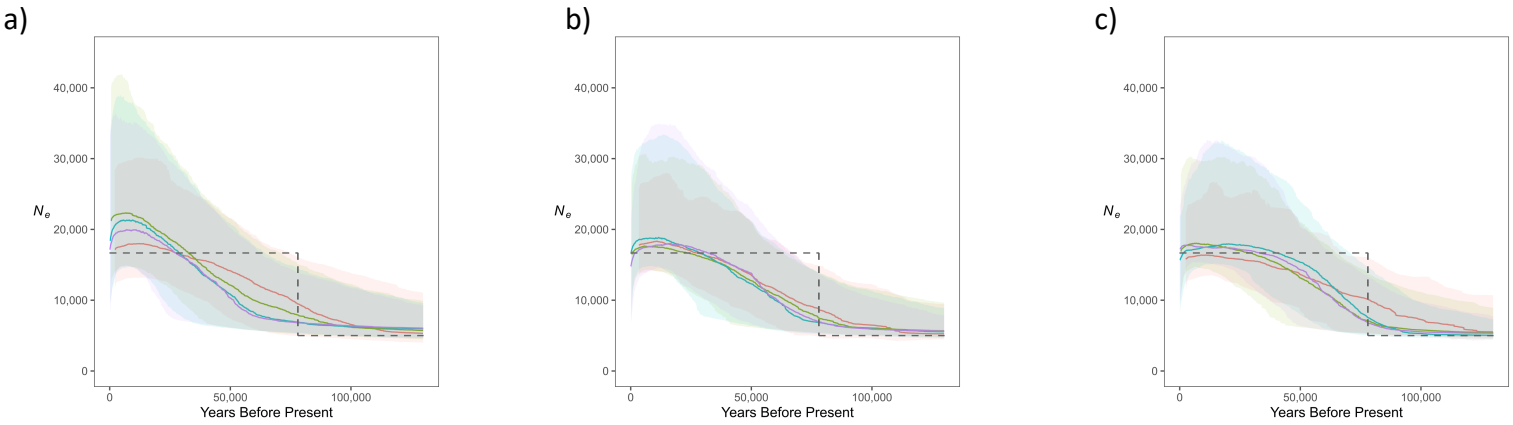

Supplementary material 5a : Variations of the effective population size (N_e) through time reconstructed by the STAIRWAYPLOT on simulated datasets of a) 1,000, b) 5,000 and c) 10,000 independent loci of 100 bp each under the NS scenario (see the main text). The true (simulated) demography is represented by the grey dotted lines. The SFS was computed on 5 (*red*), 10 (*green*), 15 (*blue*), and 20 (*purple*) diploid individuals. The median values (in bold) and the 75% confidence intervals (shaded areas) are the average of the STAIRWAYPLOT inferences performed on

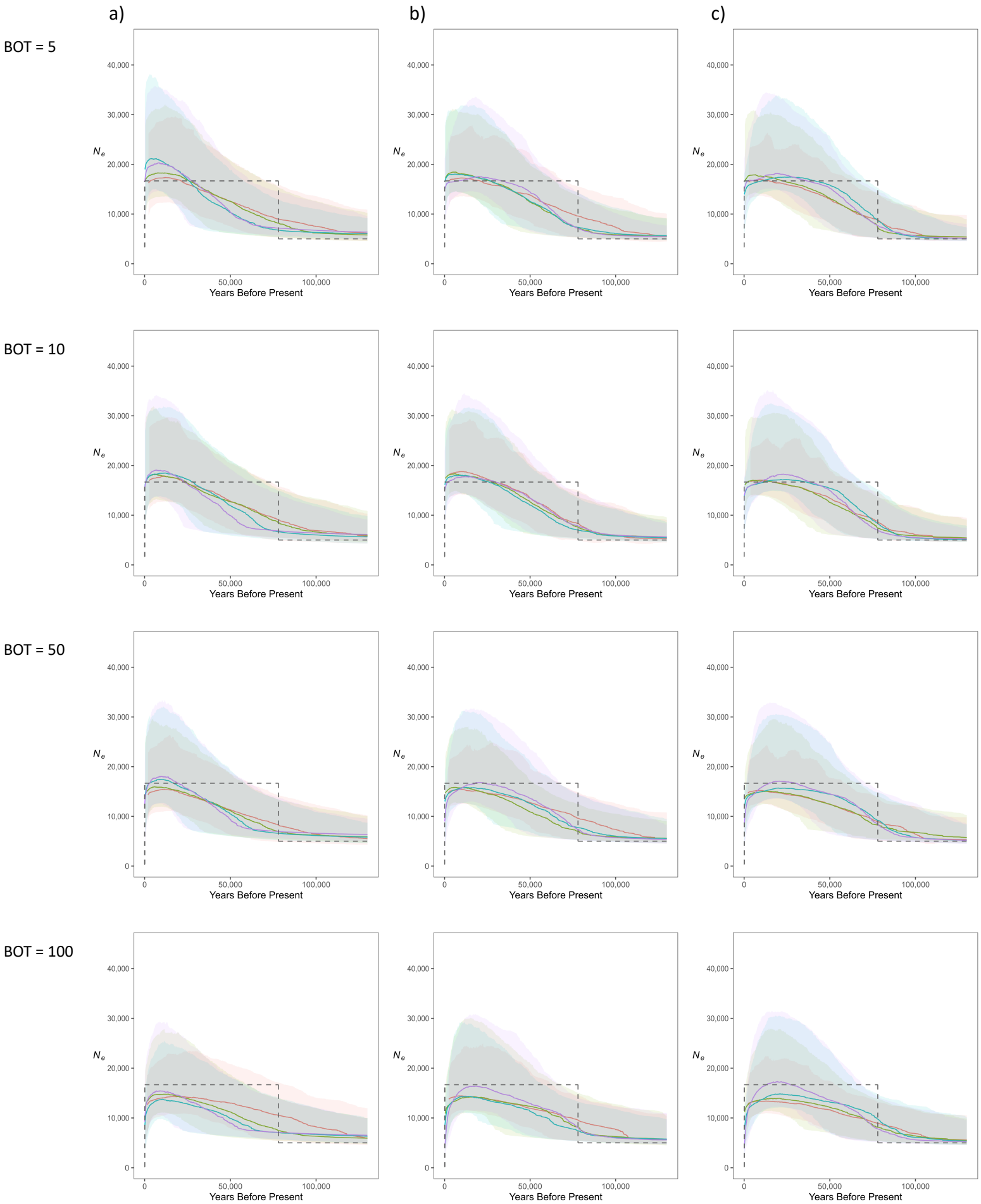

Supplementary material 5b : Variations of the effective population size (N_e) through time reconstructed by the STAIRWAYPLOT on simulated datasets of a) 1,000, b) 5,000, c) 10,000 independent loci of 100 bp each under NS_{BOT} scenarios with T_{BOT} = 5 generations (see the main text). The true (simulated) demography is represented by the grey dotted lines. The SFS was computed on 5 (*red*), 10 (*green*), 15 (*blue*), and 20 (*purple*) diploid individuals. The median values (in bold) and the 75% confidence intervals (shaded areas) are the average of the STAIRWAYPLOT inferences performed on ten independent simulated datasets.

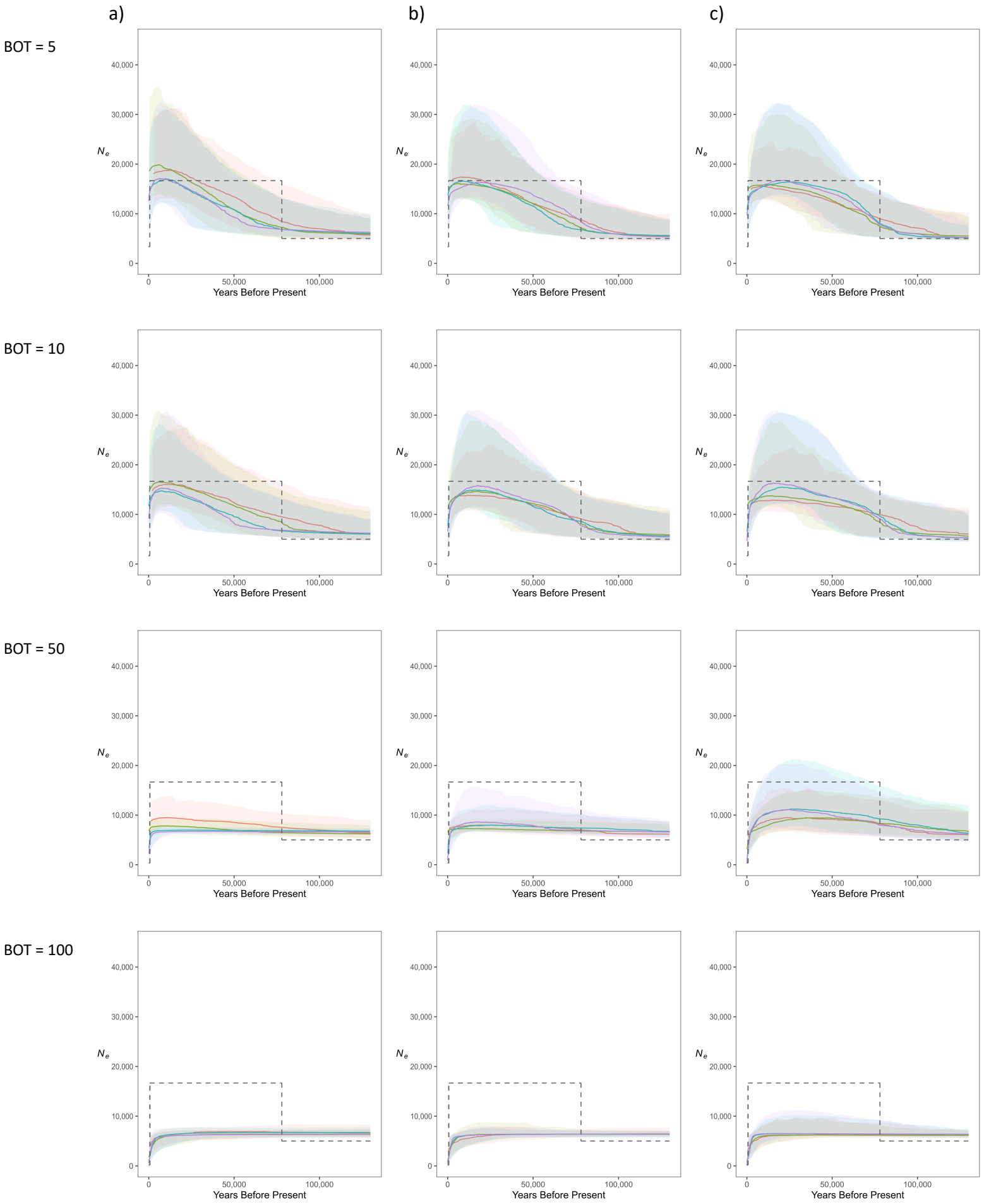

Supplementary material 5c : Variations of the effective population size (N_e) through time reconstructed by the STAIRWAYPLOT on simulated datasets of a) 1,000, b) 5,000, c) 10,000 independent loci of 100 bp each under NS_{BOT} scenarios with T_{BOT} = 50 generations (see the main text). The true (simulated) demography is represented by the grey dotted lines. The SFS was computed on 5 (*red*), 10 (*green*), 15 (*blue*), and 20 (*purple*) diploid individuals. The median values (in bold) and the 75% confidence intervals (shaded areas) are the average of the STAIRWAYPLOT inferences performed on ten independent simulated datasets.

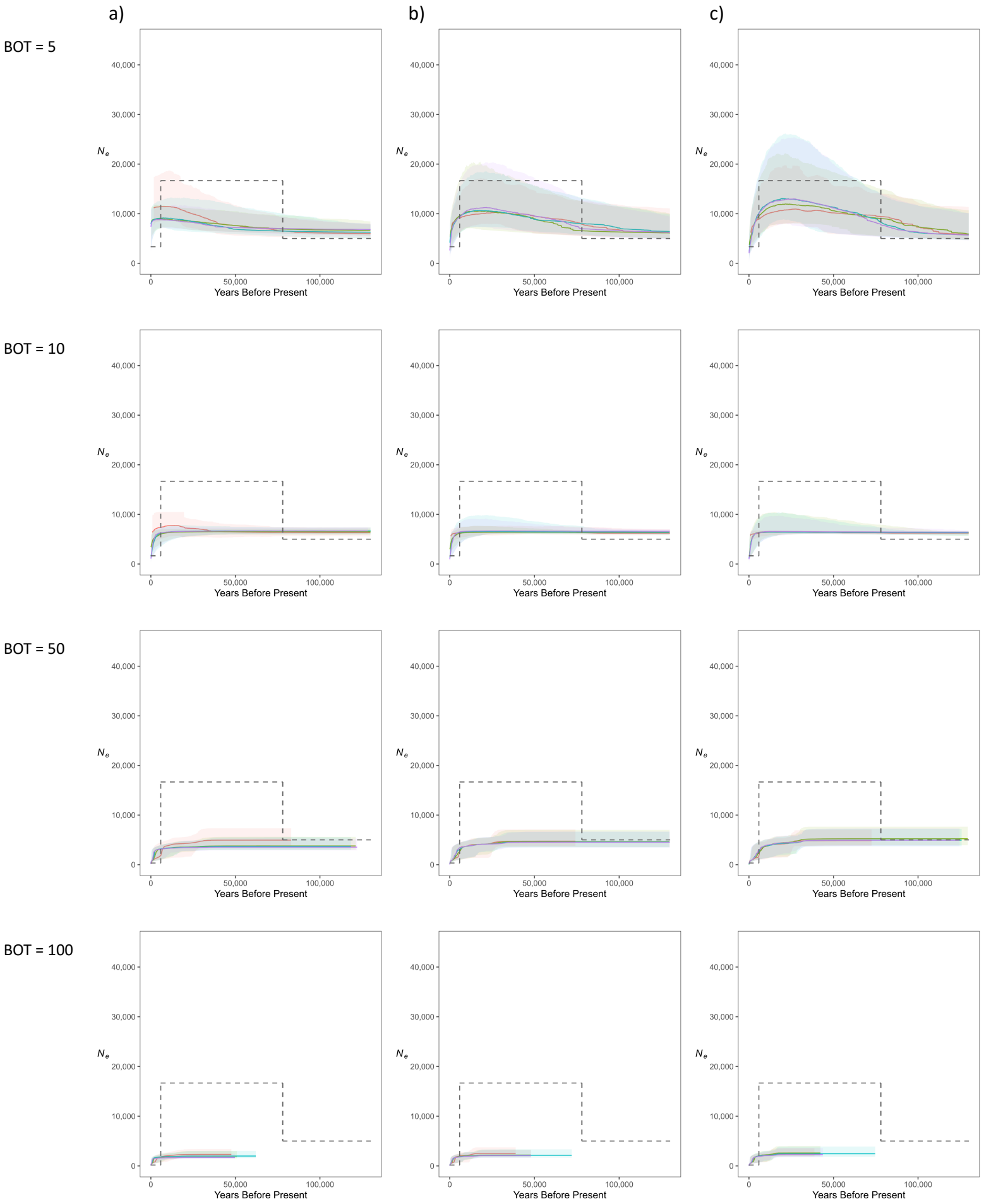

Supplementary material 5d : Variations of the effective population size (N_e) through time reconstructed by the STAIRWAYPLOT on simulated datasets of a) 1,000, b) 5,000, c) 10,000 independent loci of 100 bp each under NS_{BOT} scenarios with T_{BOT} = 450 generations (see the main text). The true (simulated) demography is represented by the grey dotted lines. The SFS was computed on 5 (*red*), 10 (*green*), 15 (*blue*), and 20 (*purple*) diploid individuals. The median values (in bold) and the 75% confidence intervals (shaded areas) are the average of the STAIRWAYPLOT inferences performed on ten independent simulated datasets.

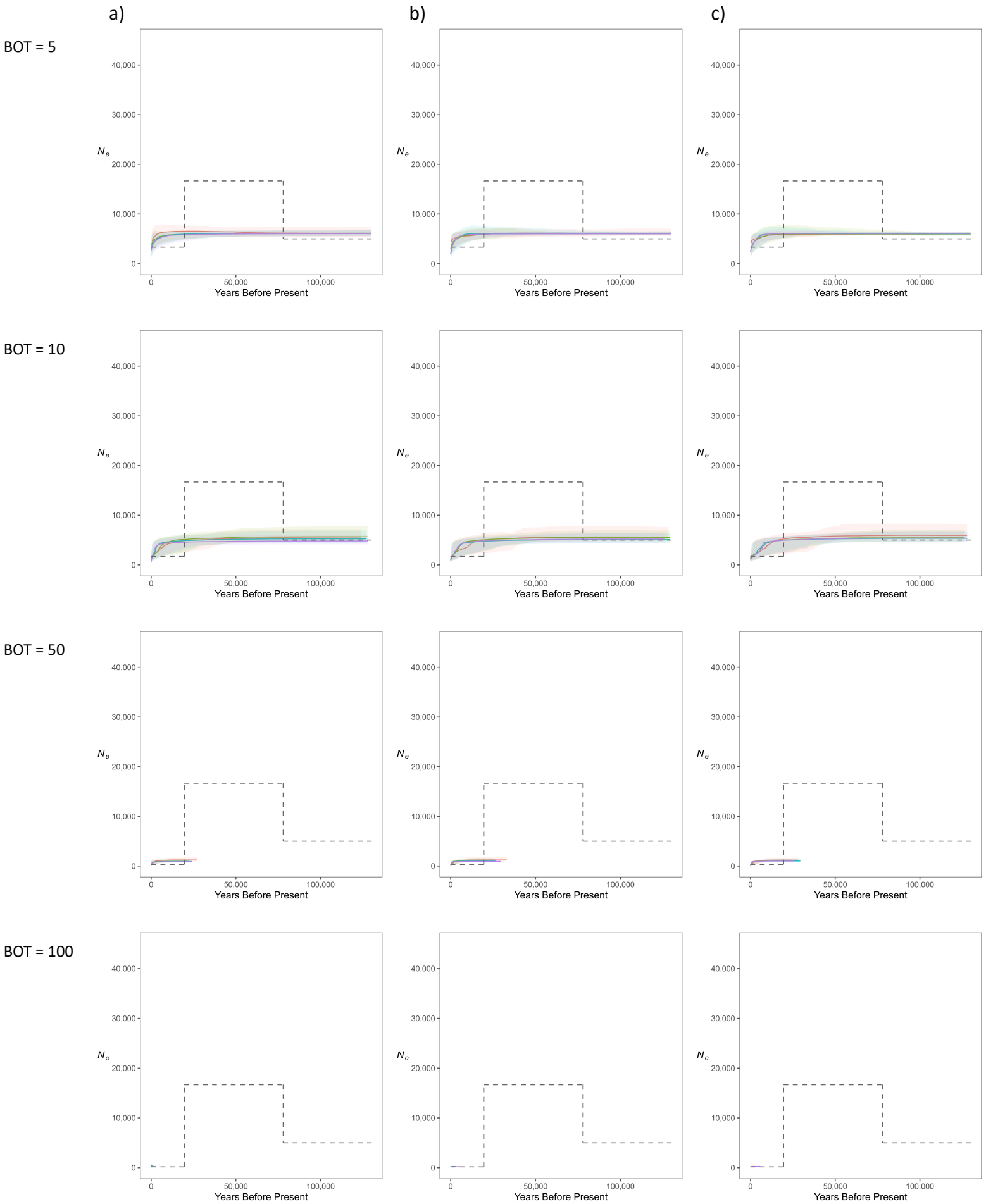

Supplementary material 5e : Variations of the effective population size (N_e) through time reconstructed by the STAIRWAYPLOT on simulated datasets of a) 1,000, b) 5,000, c) 10,000 independent loci of 100 bp each under NS_{BOT} scenarios with T_{BOT} = 1,500 generations (see the main text). The true (simulated) demography is represented by the grey dotted lines. The SFS was computed on 5 (*red*), 10 (*green*), 15 (*blue*), and 20 (*purple*) diploid individuals. The median values (in bold) and the 75% confidence intervals (shaded areas) are the average of the STAIRWAYPLOT inferences performed on ten independent simulated datasets.

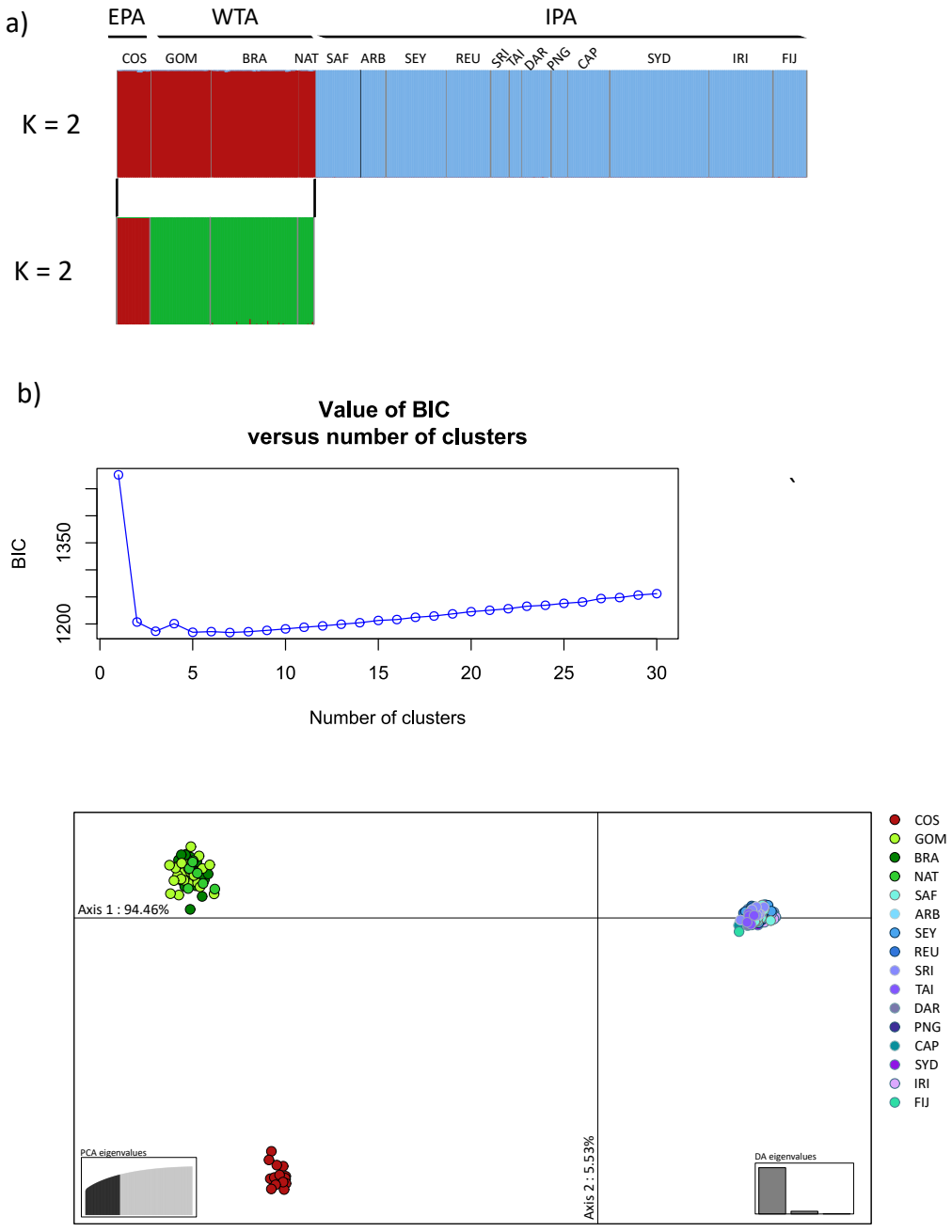

Supplementary Material 6: a) Average probability membership (y-axis) as inferred by fastSTRUCTURE in the global dataset. Only values of K maximizing marginal likelihood are shown. b) DAPC computed in the global dataset; Top: the BIC values for K ranging from 1 to 30; Bottom: scatter plot of the genotypes using the first and second discriminant components, colored according to the sampling site.

Ethics approval

All samples presented in this study were collected for alternative purposes, such as monitoring of local fisheries or biodiversity, and samples were re-used to avoid new invasive sampling. Samples from New South Wales (Australia) were collected in accordance with NSW DPI Animal Care and Ethics Committee permit 07/08 and NSW DPI Research Permit Section 37 (PO1/0059A-2.0). Sample collection in Cape York (Australia) was conducted under a CSIRO animal ethics permit (A11041; A2-2016; 2017-04). Tissue samples obtained from northern Australia, as published in Tillett et al. (2012), were collected under the S17 fisheries permit number 27134 and Kakadu permit number RK 689, in agreement with animal ethics clearance number A07001. Samples in Papua New Guinea were collected with consent from local communities in Gulf Province, and under supervision of the Gulf Provincial Fisheries Office. All fin clips from the Gulf of Mexico were collected under two IACUC protocols: one at the University of South Alabama (IACUC protocol 974394) and one at Mississippi State University (IACUC-17-620). Samples from Japan were obtained in accordance with the Guidelines for Care and Use of Animals approved by the ethics committee of the University of Tokyo (A16-13 and P19-2). The capture of Bull Sharks is permitted by the Agriculture, Forestry and Fisheries Department of Okinawa Prefecture (26-29, 27-25, 28-18, 29-20, 30-30, 31-22, 2-7). Handling of live shark specimens from Fiji were approved under the Research Permit issued by the Fiji Ministry of Education, Heritage and Arts to Beqa Adventure Divers and performed in accordance with relevant guidelines and regulations. All samples from Brazil were collected from parts of dead discarded bycatch specimens in local markets (2003-2005) under market sampling permit IBAMA PA 037/2002; samples corresponded to the same set as previously used in Karl et al. (2011) and no ethical agreement was required. Samples from Western North Atlantic (USA), Indonesia, and Thailand were collected from local fisheries landings and did not require specific ethics approvals, as per national guidelines. All material from Sri Lanka was collected from dead fisheries bycatch specimens that are not protected by the Fauna and Flora Protection Ordinance (FFPO) or any other law in place in Sri Lanka, in accordance with the letter with reference number WL/3/2/74/17, dated 4th January 2018, issued by the Department of Wildlife Conservation, Sri Lanka. Samples from the Arabian Sea and adjacent waters were collected from fishery

landings and no sampling permit was required. An authorization letter from the Ministry of Climate Change and Environment of the United Arab Emirates was obtained. Costa Rican samples were collected under the biodiversity permit VI-2391-2019 issued to the project VI-B7162. All samples from Reunion Island were collected from dead sharks caught on the Reunion Island shark control program and no ethical agreement was required. Samples from Seychelles were collected from landed artisanal fishery catch and no ethical agreement was required. All samples provided by the KZN Sharks Board from the east coast of South Africa were collected from dead sharks caught in the KwaZulu-Natal bather protection programme as constituted by Act 5 of 2008 in the province of KwaZulu-Natal and no ethical agreement was required. All shipping procedures of shark tissue samples were conducted under the relevant import and export permits issued by the Australian Government, Department of Agriculture and Water Resources. The species exported is not listed under CITES or any other international regulatory convention. Samples were imported into Australia under AQIS permit number 0001500212 and 0003253262 issued to CSIRO.